iScience

CellPress
OPEN ACCESS

Article

Identification of actionable targets for breast cancer intervention using a diversity outbred mouse model

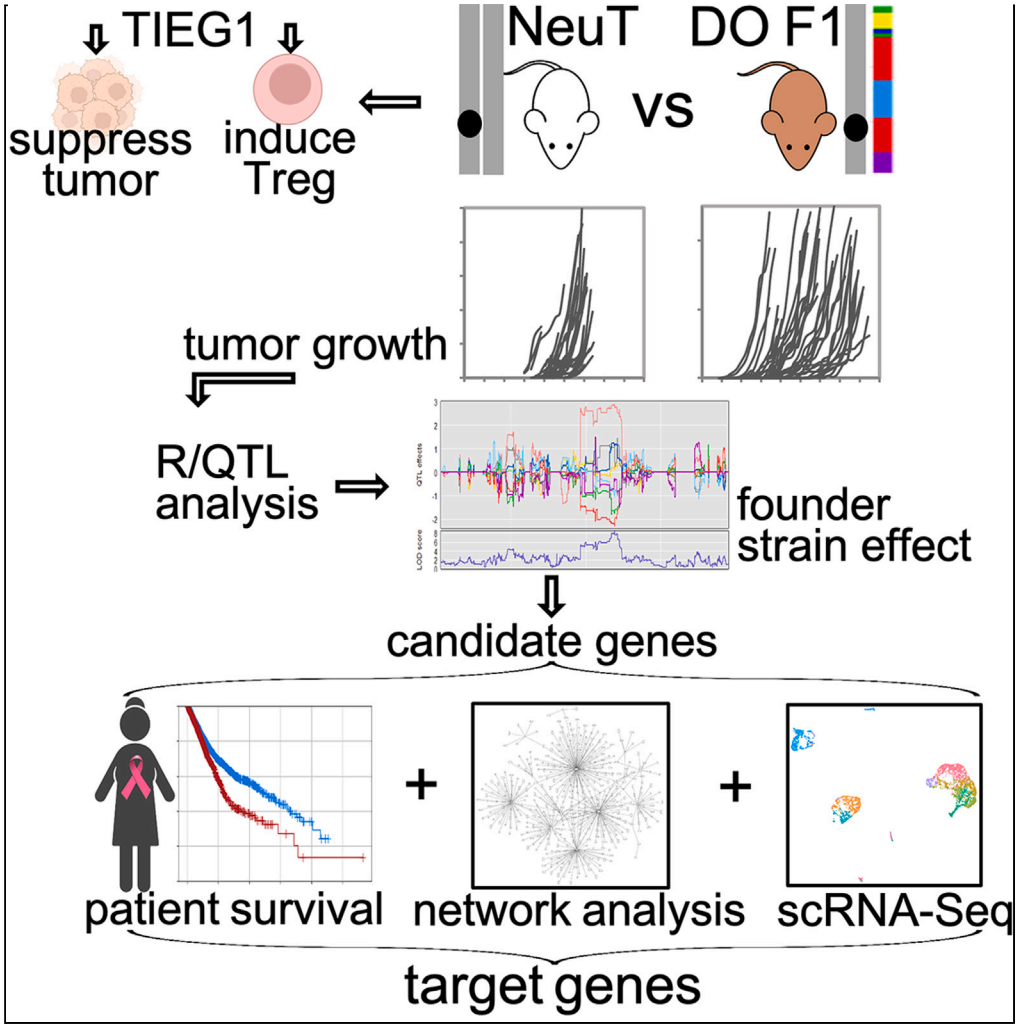

Jennifer B. Jacob, Kuang-Chung Wei, Gerold Bepler, ..., Joanne Xiu, Prahlad Parajuli, Wei-Zen Wei

weiw@karmanos.org

Highlights

HER2/Neu-expressing diversity outbred F1 mice enable genetic linkage analysis

26 Genes in 3 quantitative trait loci (QTL) predicted breast cancer survival

The myeloid checkpoint gene, LILRB4, emerged as an actionable intervention target

TIEG1 suppresses tumor growth and is critical to regulatory T cell development

Jacob et al., iScience 26, 106320
April 21, 2023
https://doi.org/10.1016/j.isci.2023.106320

iScience

CellPress
OPEN ACCESS

Article

Identification of actionable targets for breast cancer intervention using a diversity outbred mouse model

Jennifer B. Jacob,[1] Kuang-Chung Wei,[1] Gerold Bepler,[1] Joyce D. Reyes,[1] Andi Cani,[2] Lisa Polin,[1] Kathryn White,[1] Seongho Kim,[1] Nerissa Viola,[1] Julie McGrath,[3] Anthony Guastella,[3] CongCong Yin,[4] Qing-Shen Mi,[4] Benjamin L. Kidder,[1] Kay-Uwe Wagner,[1] Stuart Ratner,[1] Victoria Phillips,[1] Joanne Xiu,[3] Prahlad Parajuli,[1] and Wei-Zen Wei[1,5,*]

SUMMARY

HER2-targeted therapy has improved breast cancer survival, but treatment resistance and disease prevention remain major challenges. Genes that enable HER2/Neu oncogenesis are the next intervention targets. A bioinformatics discovery platform of HER2/Neu-expressing Diversity Outbred (DO) F1 Mice was established to identify cancer-enabling genes. Quantitative Trait Loci (QTL) associated with onset ages and growth rates of spontaneous mammary tumors were sought. Twenty-six genes in 3 QTL contain sequence variations unique to the genetic backgrounds that are linked to aggressive tumors and 21 genes are associated with human breast cancer survival. Concurrent identification of TSC22D3, a transcription factor, and its target gene LILRB4, a myeloid cell checkpoint receptor, suggests an immune axis for regulation, or intervention, of disease. We also investigated TIEG1 gene that impedes tumor immunity but suppresses tumor growth. Although not an actionable target, TIEG1 study revealed genetic regulation of tumor progression, forming the basis of the genetics-based discovery platform.

INTRODUCTION

Although major somatic drivers such as oncogenes and tumor suppressor genes have been characterized, cancer risk genes that enable somatic driver activity remain elusive.[1–3] These genes, especially immune regulatory genes, may exert a sizable impact on clinical outcome.[3] We sought such regulatory genes of breast cancer development via two complementary approaches: conventional targeted analysis and functional genomics interrogation.

A previously identified candidate cancer risk gene, TGFβ-inducible early gene 1 (TIEG1), or Krüppel-like factor 10 (KLF10), is a ubiquitously expressed transcription factor.[4,5] In the immune system, TIEG1 negatively regulates T-bet and GATA3 and promotes the transcription of TGFβ1 and Foxp3. Upon signaling, cytoplasmic TIEG1 is mono-ubiquitinated by the E3 ubiquitin ligase ITCH and marked for nuclear localization, where TIEG1 activates the Foxp3 promoter.[6,7] Foxp3 mediates the conversion of naive $CD4^+$T cells to immunosuppressive $CD4^+CD25^+$ regulatory T cells (Treg).[8] In $TIEG1^{-/-}$ mice, TIEG1-induced genes are silenced, which leads to epigenetic chromatin remodeling and impaired activation of FoxP3, and a reduction in the conversion of peripheral Treg (pTreg).[8,9] Independently, phosphorylation of Tyr179 in TIEG1 by the tyrosine kinase Tyk2 promotes non-canonical K-27-linked polyubiquitination, which inhibits nuclear translocation and blocks TIEG1 access to the Foxp3 promoter, effectively blocking Treg conversion.[10] Depletion of Treg enhances the anti-tumor activity of HER2 vaccines.[11,12] Therefore, we evaluated the role of TIEG1 as a cancer risk gene in pTreg-deficient $TIEG1^{-/-}$ mice. We further measured the development of spontaneous mammary tumors in TIEG1-deficient NeuT mice that express a transforming rat Neu.[13]

For a more comprehensive analysis, we interrogated the entire genome for regulatory genes that accelerate or impede HER2/Neu-induced spontaneous tumors. We established a functional genomics platform

[1]Department of Oncology, Karmanos Cancer Institute, Wayne State University, Detroit, MI, 48201, USA

[2]Department of Internal Medicine, Rogel Cancer Center, University of Michigan, Ann Arbor, MI, 48109, USA

[3]Clinical and Translational Research, Caris Life Sciences, Irving, TX75039, USA

[4]Department of Immunology, Henry Ford Health System, Detroit, MI48202, USA

[5]Lead contact

*Correspondence: weiw@karmanos.org

https://doi.org/10.1016/j.isci.2023.106320

of BALB NeuT mice in the diversity outbred (DO) background[14] to identify regulatory genes that accelerate or impede HER2/Neu-induced spontaneous mammary tumors. DO mice were generated by non-sibling crossing of 8 inbred founder strains (A/J, C57BL/6J, 129S1/SvlmJ, NOD/HILtJ, NZO/HiLtJ, CAST/EiJ, PWK/PhJ and WSB/EiJ) that encompass >45 million single nucleotide polymorphism (SNP), or >90% of all polymorphic alleles in laboratory and wild mice. Of the 8 founder strains, two wild mouse strains CAST/EiJ and PWK/PhJ contribute over 50% of the total SNP for genetic mapping. Because the genome of each founder strain has been fully sequenced, the genome of each DO mouse can be deduced using the Giga Mouse Universal Genotyping Array (GigaMUGA) which displays >143,000 genetic markers, mostly SNPs, distributed evenly across the 20 chromosomes. This array allows the inference of small chromosomal segments, haplotype blocks, by their inbred strain of origin. DO mice express unique polymorphic alleles with an average frequency of 12.5%, because each allele originates from one of the eight founder strains. These mice mimic humans in their genetic heterogeneity and have been used to study complex biological processes such as heart and renal function,[15,16] response to environmental toxins[17] or responsiveness to vaccination against tuberculosis.[18,19] Once the candidate genes are identified through founder haplotype effects and their clinical significance validated in human databases, DO F1 mice, or collaborative cross F1 mice[20,21] can be used for functional and therapeutics analyses.

Using DO F1 mice that express human HER2, we previously identified the MHC IB gene, H2-T23, in Chromosome 17 (Chr 17) as a key regulator of HER2 vaccine response.[22] H2-T23 harbors a stop codon alteration unique to the haplotypes that are associated with stronger HER2 immunity. H2-T23 interacts with the immune suppressive NK checkpoint molecule, NKG2A, indicating NK cells are regulators of HER2 vaccine response. Indeed, HER2 vaccine response was reduced in NK depleted mice. Our successful identification of an NK checkpoint ligand that regulates HER2 vaccine response supports the feasibility of this approach to define regulatory genes of cancer progression.

In this study, we performed functional genomics in DO F1 NeuT mice that express a transforming rat Neu and develop spontaneous mammary tumors to discover quantitative trait loci (QTL) that regulate breast cancer progression. We established a progressive selection process to identify candidate genes with unique genetic alterations associated with accelerated tumor onset age or growth rate, validated their clinical relevance with large cohorts of primary and metastatic breast cancer patients, selected genes with shared functional pathways and defined the cell types expressing the target genes by single cell RNA analysis. Through complementary cancer biology and bioinformatics analyses, we have identified genes that can pave the way to innovative cancer interventions.

RESULTS

Neu oncogene expression in spontaneous mammary tumors visualized by ImmunoPET imaging

Syngeneic BALB NeuT female mice express a transforming rat Neu (NeuT) and develop spontaneous mammary tumors in up to 10 mammary fat pads, designated by fat pad numbers 1–10 (Figure 1A). Neu is the rat homolog of human HER2, and NeuT mice harbor a transmembrane mutation (V664E) that confers constitutive activity.[23] A computed positron emission tomography, computed tomography (PET/CT) scan of a representative BALB NeuT female showed tumors in all 10 mammary fat pads ranging in size from 3 × 4mm (18 mm^3) to 6 × 8mm (144 mm^3) (Figure 1B and 1C). Expression of the NeuT oncogene was assessed by immunoPET imaging using [^{64}Cu]Cu-NOTA-α-Neu ($t_{1/2}$~ 12.7 h). The radiotracer was preferentially retained in the mammary tumors, as control tumor-free mice did not show fat pad retention. There was minimal non-specific binding in healthy tissues with the exception of the liver and bladder (Figure 1C), where the tracer was processed for excretion.[24] Control [^{64}Cu]Cu-NOTA-IgG treatment of tumor-bearing mice showed non-specific uptake in the peritoneal cavity, but no accumulation in the tumors (FigureS1).

Using ASIPro VMTM software (Concorde Microsystems), volumes of interest (VOI) in the PET image were measured on various planar sections of the acquired image. The mean VOI was calculated and expressed as % injected dose per gram of tissue (% ID/g). The % ID for the 10 tumors in Figure 1C for [^{64}Cu]Cu-NOTA-α-Neu totaled ~60%, showing preferential retention of [^{64}Cu]Cu-NOTA-α-Neu, in the tumors. These results affirmed consistent expression of the Neu oncogene that drives mammary tumor progression. Expression of Neu was further verified by flow cytometric analysis of enzymatically dissociated tumor cell to show Neu expression in ~65% of CD45 negative cells (Figure 1D).

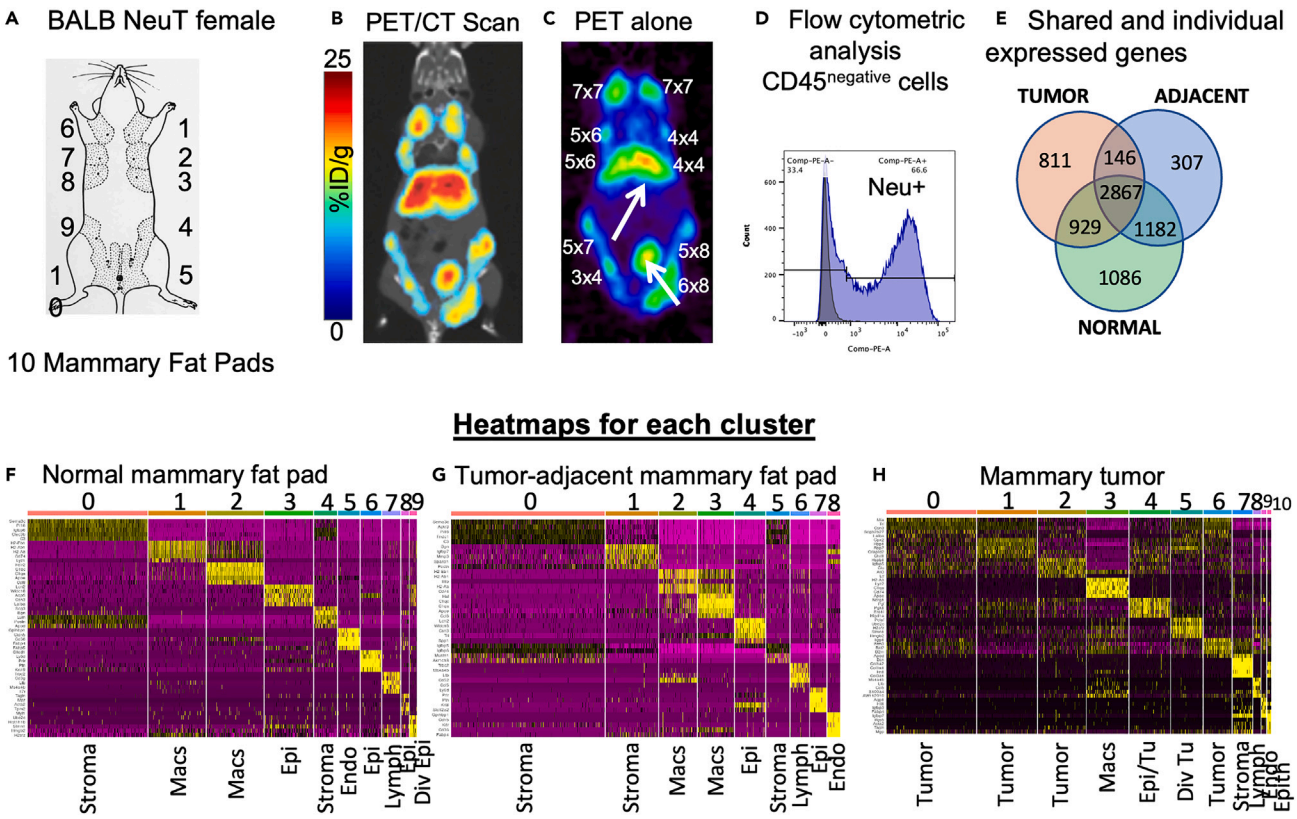

Figure 1. Characterization of spontaneous mammary tumor progression in BALB NeuT mice

(A) BALB NeuT mice develop tumors in all 10 mammary fat pads, numbered 1–10.

(B) PET/CT scan of a BALB NeuT female.

(C) PET imaging with [^{64}Cu]Cu-NOTA-α-neu probe (clone 7.16.4) showing tracer accumulation in tumors of varying sizes. White arrows indicate liver and bladder.

(D) Flow cytometric analysis of Neu expression in CD45-negative cells from a dissociated NeuT mammary tumor.

(E) Venn diagram utilizing Venny (https://www.biotools.fr/misc/venny) depicts shared and unique genes in mammary tissue.

(F–H) scRNA-Seq analysis of (F) normal, (G) tumor-adjacent, and (H) tumorous mammary tissues. Yellow indicates genes with the highest copy numbers.

Single cell transcriptomic analysis of BALB NeuT mammary tissues

To fully characterize the cellular composition, single cell RNA sequencing (scRNA-Seq) was performed with enzymatically dissociated mammary tumors and tumor-adjacent fat pad tissues from 17-week old BALB NeuT female mice. In parallel, normal mammary fat pads from 9-week-old NeuT females were analyzed. A total of 6064, 4502 and 4753 genes were identified in the normal, tumor-adjacent, and tumor tissues, respectively (Figure 1E). Forty percent of the genes were shared by all three mammary tissues (2867), whereas tumor adjacent tissue expressed fewer unique genes (307) compared with normal (1086) or tumor tissue (811).

The R-package Seurat (v 4.0.6) was used to normalize and scale the data.[25,26] Differentially expressed genes were identified for each cluster and heatmaps for the top 5 genes based on fold change were generated (Figure 1F–1H). The Tabula Muris database (https://tabula-muris.ds.czbiohub.org/) was queried for the 5 genes with the highest counts to determine the identity of each cluster. There were 9, 8, and 10 cell clusters in the normal, tumor-adjacent and tumorous mammary fat pads, respectively. The cell clusters are indexed as 0–10 with cluster 0 containing the greatest number of cells. All three samples contained 5 major cell types: stromal, myeloid/macrophage, endothelial, lymphoid and epithelial/tumor cells (Figures 1F–1H). Tumor cells occupied the bulk of the tumor mass to include 5 cell clusters (Figure 1H). In tumor-adjacent mammary fat pad, stromal cells and myeloid/macrophages were the primary cell types and included 2 distinct epithelial cell clusters. In normal mammary tissue, stromal and myeloid/macrophages also made up the major cell types and included 4 epithelial cell clusters.

Development of spontaneous mammary tumors in TIEG1-deficient mice

We tested if manipulation of TIEG1 alters anti-tumor immunity using B6 HER2 Tg mice that express the human ERBB2 (HER2) as a self-antigen,[27] but do not develop spontaneous mammary tumors.[28] C57BL/6 (B6) TIEG1$^{-/-}$ mice were crossed with B6 HER2 Tg mice to generate TIEG1$^{+/-}$ HER2 Tg mice which were backcrossed with TIEG1$^{-/-}$ mice to generate B6 TIEG1$^{-/-}$ HER2 Tg mice. TIEG1 deficient mice were randomized and electro-vaccinated with pE2TM encoding the extracellular and transmembrane domains of human HER2 (Figure 2A). Production of IFN-γ-secreting T cells was significantly higher in B6 TIEG1$^{-/-}$ HER2 mice (mean ± SD, 15 ± 2) over their B6 TIEG1$^{+/+}$ HER2 littermates (7 ± 1)($p< 0.01$), verifying greater immune reactivity to HER2 in TIEG1$^{-/-}$ mice (Figure 2B). Loss of TIEG1 also resulted in a significantly enhanced α-HER2 T cell response in wild type B6 mice that recognize HER2 as a foreign antigen (TIEG1$^{-/-}$ 355 ± 83, TIEG$^{+/+}$ 172 ± 25) ($p = 0.05$) (Figure 2C). The growth of transplanted HER2^{+} E0771 mammary tumors were delayed, with 40% of TIEG1$^{-/-}$ HER2 Tg mice remaining tumor-free 5 weeks after all TIEG1$^{+/-}$ HER2 littermates developed palpable tumors ($p< 0.05$)[29] (Figure 2D). Therefore, removal of TIEG1 resulted in enhanced HER2 immunity and reduced tumor growth, consistent with its role in pTreg generation.

We proceeded to test if the development of spontaneous mammary tumors were similarly delayed in TIEG1$^{-/-}$, pTreg-deficient mice. Because HER2 Tg mice do not develop mammary tumors, we crossed BALB NeuT mice with B6 TIEG1$^{-/-}$ mice to generate (BALBxB6) TIEG1$^{+/-}$ NeuT mice, which were backcrossed with B6 TIEG1$^{-/-}$ mice to generate (BALBxB6) TIEG1$^{-/-}$ NeuT mice. The median tumor-free survival of (BALBxB6) TIEG1$^{-/-}$ NeuT mice was 21 weeks of age (woa) (Figure 2E, *gray diamonds*) compared to 26 woa in their TIEG1 intact (BALBxB6) NeuT littermates (Figure 2E, *black squares*). Control BALB NeuT mice developed tumors with median tumor-survival age of 16 woa as expected (Figure 2E, *open circle*). Loss of TIEG1 in the test mice was verified by qPCR (Figure 2F). We conclude that introduction of the B6 genetic background delayed tumor onset age, but loss of TIEG1 accelerated the development of spontaneous mammary tumors.

Accelerated tumor onset in (BALBxB6) TIEG1$^{-/-}$ NeuT mice suggested a loss of other critical TIEG1 functions, such as tumor suppressor activity,[30,31] so that tumors appeared early even though anti-tumor immunity was elevated. scRNA-Seq analysis revealed that expression of TIEG1 (Klf10 gene) was nearly ubiquitous in mammary tumor tissues (Figures 2G/2H, *top panels*), except for lymphocytes which express CD3d but not TIEG1 (Figures 2G and 2H, *bottom panels*). Thus, the tumor suppressor activity of TIEG1 may prevail over pTreg activity,[32] such that (BALBxB6) TIEGF1$^{-/-}$ NeuT mice showed accelerated tumor progression despite pTreg depletion and elevated tumor immunity.

Importantly, the observation that tumor onset was delayed on introduction of the B6 genetic background suggested yet undefined regulatory mechanisms of mammary tumor progression. We sought to reveal such regulatory genes by expressing NeuT in DO mice that are specifically designed for genetic linkage analysis.[14]BALB NeuT mice were crossed with individually unique DO mice to generate (BALBxDO) F1 NeuT mice so that one chromosome originated from the BALB NeuT parent and the other chromosome was a mosaic of the 8 founder strains.[22,33,34] The unique, yet thoroughly defined, genetic composition of each mouse is the basis for genetic linkage analysis and the identification of QTLs that regulate tumor growth traits.

Mammary tumor progression in (BALBxDO) F1 NeuT mice

We monitored the spontaneous tumor onset age, location, multiplicity, and growth rate in (BALBxDO) F1 NeuT mice. Palpable tumors appeared in control BALB NeuT females at 14–19 woa (Figures 3A and 3B). Tumors appeared in (BALBxDO) F1 NeuT females more variably, with onset age ranging from 9 to 23 weeks. Also, (BALBxDO) F1 NeuT female mice developed tumors in 8.7 ± 1 fat pads which is significantly higher than the tumors in BALB NeuT female mice (7.4 ± 1.2 fat pads) ($p< 0.001$) (Figure 3C). Tumors appeared in any of the 10 mammary fat pads in either BALB NeuT or (BALBxDO) F1 NeuT female mice.

In BALB NeuT male mice (Figure 3D, *left*), salivary tumors arose around 7 months of age with 100% penetrance and mammary tumors appeared sporadically (1.04 + 0.2SEM). Of interest, (BALBxDO) F1 NeuT males (Figure 3D, *right*) developed mammary tumors more frequently (3 ± 1.2 SEM) ($p = < 0.0001$), and the incidence of salivary tumors was greatly reduced (1/22). In both BALB NeuT and (BALBxDO) F1 NeuT males, mammary tumors occurred primarily in the thoracic fat pads (#1–3 and #6–8), with few occurring in the inguinal fat pads (#4–5 and #9–10). This contrasted with female mice that consistently developed mammary tumors in both inguinal and thoracic mammary fat pads. Although all fat pads are composed of white adipose tissue, there may be distinctions between thoracic and inguinal fat pads that influence

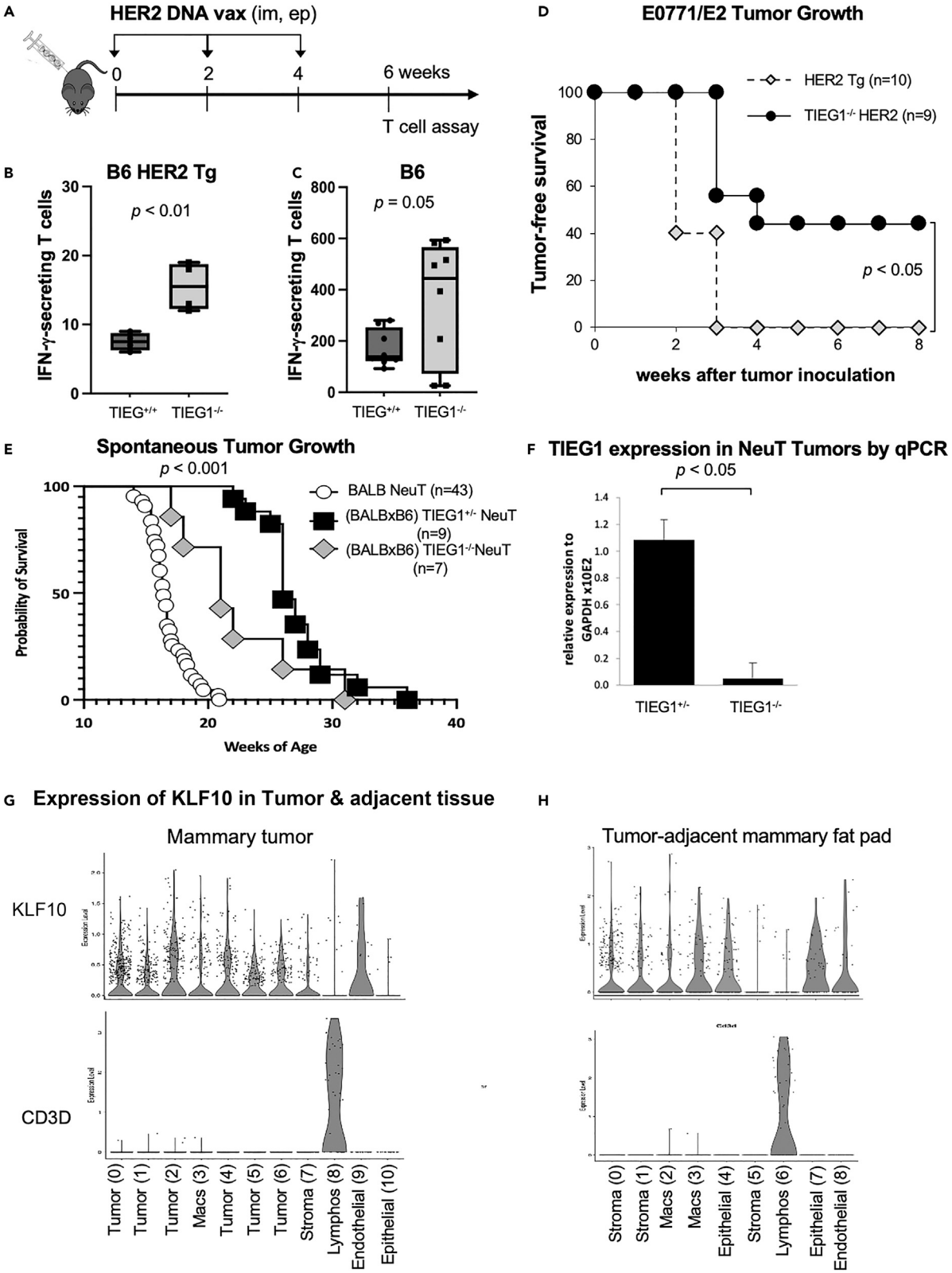
A
HER2 DNA vax (im, ep)
0
2
4
6 weeks
T cell assay
B
B6 HER2 Tg
p < 0.01
IFN-γ-secreting T cells
TIEG+/+
TIEG1-/-
C
B6
p = 0.05
IFN-γ-secreting T cells
TIEG+/+
TIEG1-/-
D
E0771/E2 Tumor Growth
HER2 Tg (n=10)
TIEG1-/- HER2 (n=9)
Tumor-free survival
p < 0.05
weeks after tumor inoculation
E
Spontaneous Tumor Growth
p < 0.001
BALB NeuT (n=43)
(BALBxB6) TIEG1+/- NeuT (n=9)
(BALBxB6) TIEG1-/-NeuT (n=7)
Probability of Survival
Weeks of Age
F
TIEG1 expression in NeuT Tumors by qPCR
p < 0.05
relative expression to GAPDH x10E2
TIEG1+/-
TIEG1-/-
G
Expression of KLF10 in Tumor & adjacent tissue
Mammary tumor
KLF10
CD3D
Tumor (0)
Tumor (1)
Tumor (2)
Macs (3)
Tumor (4)
Tumor (5)
Tumor (6)
Stroma (7)
Lymphos (8)
Endothelial (9)
Epithelial (10)
H
Tumor-adjacent mammary fat pad
Stroma (0)
Stroma (1)
Macs (2)
Macs (3)
Epithelial (4)
Stroma (5)
Lymphos (6)
Epithelial (7)
Endothelial (8)

Figure 2. TIEG1 regulates tumor immunity and tumor growth. Tumor growth was monitored using Kaplan-Meier tumor-free survival. $p < 0.05$ was considered significant.

(A) C57BL/6 mice and C57BL/6 HER2 Tg mice with (n = 10) or without TIEG1 (n = 9) were electrovaccinated with pE2TM.

(B and C) IFN-γ producing T cells were measured by ELISPOT assay. Data are represented as the average and SD in box and whisker plots.

(D) Growth of implanted E0771/E2 tumor in HER2 Tg mice with or without TIEG1.

(E) Onset age of spontaneous tumors in NeuT mice with or without TIEG1 (n = 9 and 7, respectively).

(F) TIEG1 expression measured by qPCR. Data are represented as pooled averages +/− SEM.

(G and H) TIEG1/Klf10 (*top panels*) and Cd3d (bottom panel) expression measured by scRNA sequencing.

mammary tumor development in male mice.[35] Taken together, heritable factors strongly influenced tumor onset age and location.

Identification of QTL that regulate tumor onset age in (BALBxDO) F1 NeuT mice

To identify genes that regulate HER2/neu oncogenesis, we defined the QTL associated with mammary tumor onset age and growth rate in (BALBxDO) F1 NeuT female mice. The haplotype profile of each mouse was determined by GigaMUGA.[14] From 86 female (BALBxDO) F1 NeuT mice, over 10 million haplotype calls were made and depicted as A-H to represent the 8 founder strains (Table S1). Individual mouse genomes can be deduced through the inference of haplotype blocks according to their inbred strain of origin because the genomes of the 8 founder strains have all been fully sequenced. The frequency of haplotype calls for each founder strain averaged at the expected value of 12.5% (ranging from 11.4–13.5%), substantiating the accuracy of the analysis process. The genomic uniqueness of each mouse was calculated and displayed as the kinship matrix using the R-based R/QTL software package (https://github.com/rqtl/qtl2).[36] A kinship value of 1 (*white*) depicts complete identity to self, and 0 (*red*) means no genetic relatedness (Figure 4A). The color shades between red and white indicate degrees of relatedness. A cohort of 86 mice with minimal relatedness was subjected to DO QTL analysis.

The association between spontaneous tumor onset age and genetic markers was calculated using the R/QTL package and the LOD values at each genetic marker was presented in the genome scan Manhattan plot (Figure 4B). Distinct LOD peaks or QTL were found in Chr 1 and Chr X (Figure 4B, *arrows*). Chr 1 QTL (LOD = 8.6) was located at Chr 1:119,277,480 with a 95% confidence interval (CI) of 117,018,781-121,325,220. In Chr X, two narrow peaks were identified at 140,885,460 (CI: 139,906,385-140,930,420) (LOD = 8.0) and 140,934,630 (CI: 140,932,209-141,948,840) (LOD = 7.8).

Figure 4C/4D (*upper panels*) show the founder strain effect at each marker with the specific color designation of each founder strain. Positive values indicate longer than the average tumor latency period or later tumor onset, and negative values indicate earlier tumor onset. The corresponding genome scan Manhattan plots for Chr 1 and Chr X are shown directly below the founder strain effect plot (Figures 4C/4D, *lower panels*). In the Chr 1 QTL, the PWK haplotype drove early tumor onset (negative value, red line), followed by CAST (green line) (Figure 4C). On the other hand, late tumor onset was associated with the 129 haplotypes (positive QTL effect, salmon line). In Chr X (Figure 4D), the peak LOD region also depicted the PWK haplotype as the primary driving haplotype for early tumor onset, followed by CAST. In the Chr 1 QTL, longer latency of tumor onset age was associated with 129/S1 haplotype and in Chr X QTL, the WSB haplotype was the driver for later tumor onset.

Identification of QTL that regulate the growth rate of (BALBxDO) F1 NeuT mammary tumors

To identify the QTL that regulate the rate of tumor growth, the sum of all tumor volumes was calculated for each mouse and a differential equation used to model the dynamical behavior[37] of the tumor growth in time: $dV(t)/dt = c_1 V(t) + c_2 f(t)$. In short, the logarithm transformation of tumor volume renders a set of equations to decipher the tumor growth characteristics which is embedded in c_1 and subject to subsequent analysis. Figure 4E shows the histogram distribution of c_1 (the tumor growth rate of logarithmic tumor volume) from the 86 (BALBxDO) F1 NeuT female mice. The c_1 values were used in subsequent QTL analysis.

The association between c_1 and all genetic markers was analyzed using R/QTL and LOD values and shown in the genome scan Manhattan plot (Figure 4F). The most prominent peak (LOD = 6.7) was found at Chr 10:53,548,480 (CI: 46,307,095-54,362,980). The founder strain effect plot shows PWK (red line), CAST (green line) and WSB (purple line) haplotypes driving the highest c_1 or fastest growth rate (positive value) (Figure 4G). Therefore, PWK and CAST haplotypes were associated with both early tumor onset and faster tumor growth.

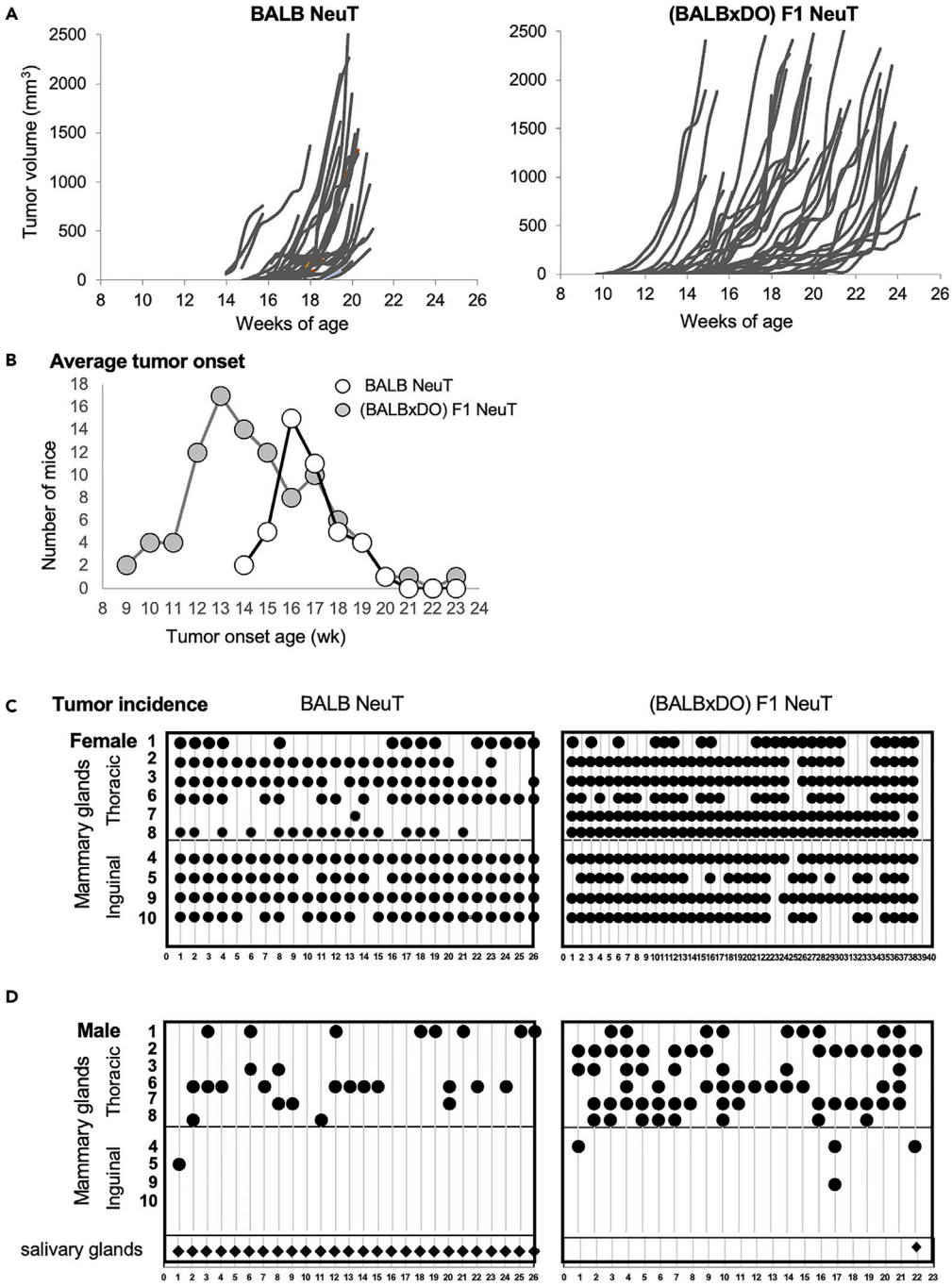

Figure 3. Development of spontaneous tumors in (BALBxDO) F1 mice

(A) Development of mammary tumors in representative BALB NeuT and (BALBxDO) F1 NeuT mice.

(B) The tumor onset age in BALB NeuT (*open circles*) and (BALBxDO) F1 NeuT mice (*gray circles*). Data are represented as pooled averages at each time point.

(C) Tumor multiplicity in female BALB NeuT and (BALBxDO) F1 NeuT mice.

(D) Tumor multiplicity in male BALB NeuT and (BALBxDO) F1 NeuT mice. Thoracic mammary glands are designated #1, 2, 3, 6, 7, 8 and the inguinal glands are #4, 5, 9, 10. Diamonds indicate the presence of salivary tumors.

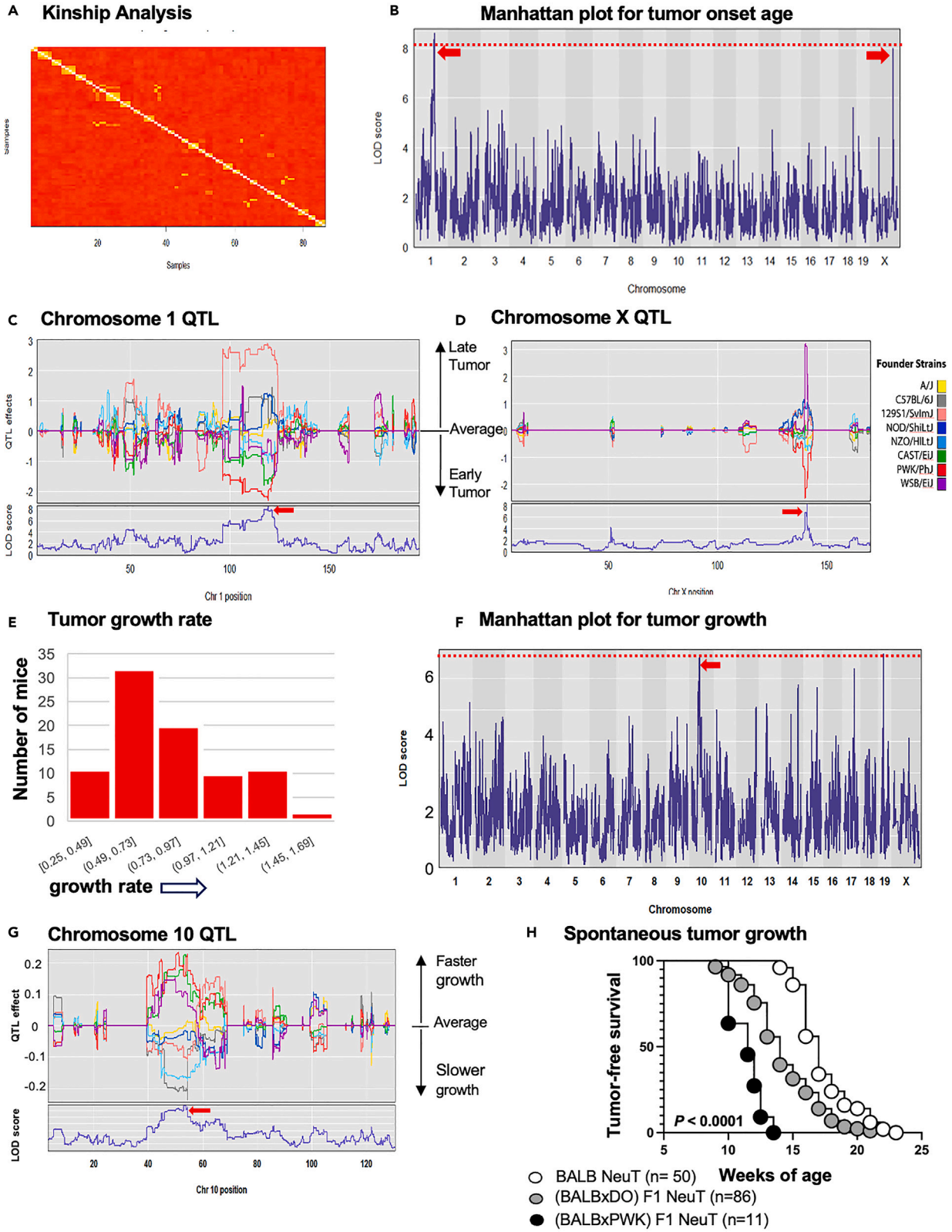
A
Kinship Analysis
Samples
B
Manhattan plot for tumor onset age
LOD score
Chromosome
C
Chromosome 1 QTL
QTL effects
LOD score
Chr 1 position
Late Tumor
Average
Early Tumor
D
Chromosome X QTL
Chr X position
Founder Strains
A/J
C57BL/6J
129S1/SvImJ
NOD/ShiLtJ
NZO/HlLtJ
CAST/EiJ
PWK/PhJ
WSB/EiJ
E
Tumor growth rate
Number of mice
[0.25, 0.49]
(0.49, 0.73]
(0.73, 0.97]
(0.97, 1.21]
(1.21, 1.45]
(1.45, 1.69]
growth rate
F
Manhattan plot for tumor growth
LOD score
Chromosome
G
Chromosome 10 QTL
QTL effect
LOD score
Chr 10 position
Faster growth
Average
Slower growth
H
Spontaneous tumor growth
Tumor-free survival
P < 0.0001
Weeks of age
BALB NeuT (n= 50)
(BALBxDO) F1 NeuT (n=86)
(BALBxPWK) F1 NeuT (n=11)

Figure 4. QTL analysis in (BALBxDO) F1 NeuT mice

(A–D) Tumor onset age was analyzed for 86 (BALBxDO) F1 NeuT mice.

(A) Kinship analysis among the 86 test mice.

(B) Manhattan plot showing two prominent QTL in Chr 1 and Chr X, respectively (*red arrows*).

(C) Founder strain effect in (C) Chr 1 and (D) Chr X. *Upper panels* show founder strain effects, with positive values indicating tumor onset age later than average (value = 0) and negative numbers indicating the opposite. *Lower panels* are the LOD score of the designated chromosome.

(E) Histogram showing the slope (c_1) of exponential tumor growth of the 86 (BALBxDO) F1 NeuT mice.

(F) Manhattan plot of QTL associated with the tumor growth rate. Arrow indicates peak at Chr 10.

(G) Founder strain effect of Chr 10 shown in the *upper panel*, where faster tumor growth is above the average and slower tumor growth is below the average. LOD peaks are shown in the *lower panel*.

(H) Tumor-free survival of (BALBxPWK) F1 NeuT mice (*black circles*, n = 11), BALB NeuT (*white circles*, n = 50) or (BALBxDO) F1 NeuT mice (*gray circles*, n = 86). Significance between groups was compared using the logrank test. $p = 0.0001$ was observed between all groups.

Onset and treatment response of spontaneous mammary tumors in (BALBxPWK) F1 NeuT mice

DO QTL analysis of (BALBxDO) F1 NeuT mice revealed that PWK and CAST were the driving haplotypes for accelerated tumor onset (Chr 1 and Chr X) and growth rate (Chr 10). We proceeded to test the hypothesis that introduction of the PWK genetic background into NeuT mice would accelerate mammary tumor development. BALB NeuT males were crossed with PWK females and tumor growth in (BALBxPWK) F1 NeuT mice was monitored. In the F1 mice, palpable tumors appeared at 10–13 woa (Figure 4H, *black circles*) that was about 4–5 weeks earlier than the onset of syngeneic BALB NeuT tumors ($p < 0.001$) (Figure 4H, *white circles*). By 14 weeks of age, all (BALBxPWK) F1 NeuT females had developed palpable tumors, whereas only half of (BALBxDO) F1 NeuT mice did (Figure 4H, *gray circles*) and none of the BALB NeuT mice had tumors at that age, validating PWK as the haplotype for accelerating HER2/Neu tumor development.

Polymorphism of genes in QTL

Toward identifying the genes that contribute to tumor progression, 173 genes were located within Chr 1 (n = 59), Chr X (n = 21) and Chr 10 (n = 93) QTL (UCSC Genome Browser Gateway, GRCm38/mm10 assembly) (https://genome.ucsc.edu/cgi-bin/hgGateway). Using Sanger Mouse Genome Project Release REL-1505 (http://www.sanger.ac.uk/sanger/Mouse_SnpViewer), we screened the genes in each QTL with LOD scores above 6.0. We identified genes that harbor missense mutations or critical insertions/deletions (Indel) unique to tthe PWK/CAST haplotypes (Table S2). This selection process resulted in 28 candidate genes: twelve genes in Chr 1, two in Chr X, and fourteen in Chr 10 (Table S2). The predicted protein changes were designated as 'conserved', when the protein maintained a similar polarity or hydrophobicity, or 'non-conserved' that could result in altered protein function. Three insertions were also identified, an in-frame insertion in EPB41L5 (Chr 1), and 2 out-of-frame insertions in RBM41 (Chr X) and NUS1 (Chr 10) which are predicted to lead to truncated proteins (https://web.expasy.org/translate/). In GP49A (Chr 10), an SNP is predicted to result in a premature STOP codon (Table S2). The remaining SNP are predicted to result in amino acid substitutions with changes in steric effects, polarity and (or) hydrophobicity.

Human genes corresponding to mouse Chr 1 and X QTL are located in human Chr 2:118,090,736-121,820,449 and human Chr X:107,021,964-109,132,432, respectively, and in the same orientation. Homologous human genes for mouse Chr 10 QTL are found in human Chr 6:101,181,257-119,349,761 in the opposite direction, except for LILRB4A that is in human Chr 19 (Figure 6A). Human homologues for NEPN and GP49A (mouse Chr 10) have not been identified. Therefore 26 of 28 genes identified through DO R/QTL analysis were found in the human genome.

Clinical indication of candidate genes

We interrogated the clinical significance of candidate genes identified in human Chr 2, Chr X, Chr 6 and Chr 19 (Table S2) by analyzing their association with breast cancer outcome using the Real World Outcomes data (Caris Life Sciences).[38] The analysis was conducted in a cohort of 3,533 women with primary breast cancer and a second cohort of 4,870 women with metastatic breast cancer. Whole transcriptome sequencing was performed with mRNA isolated from formalin-fixed paraffin-embedded tumor samples using the Illumina NextSeq 600 platform (Illumina, Inc., San Diego, CA) in a CAP-accredited, CLIA certificated laboratory (Caris Life Sciences). 'Event-free days', or real world overall survival (rwOS), was defined as the number of days from tissue collection to the first determination of tumor recurrence/metastatic progression or last contact with individual patients, whichever was earlier. Patient death was assumed for any patient without

a claim for more than 100 days, which held true for more than 95% of patients with a recorded death in the National Death Index (NDI).[39] Significant differences in event-free days between the patient populations whose gene expressions were above or below the median value were considered a validation of regulatory gene activity. "Favorable" and "adverse" genes were defined by the correlation of increased gene expression with longer or shorter event-free days, respectively. We queried the de-identified datasets using CODEai, a clinic-genomic data platform that integrates patients' molecular data with cancer treatment and clinical outcome information obtained from insurance claims data.[40] Bonferroni correction for multiplicity was performed and $p < 0.05$ was the criteria for significance.

Median expression levels for most genes were highly similar between the primary and metastatic breast cancer cohorts, differing by less than 10% (Table S3). The expression levels of 21 of the 26 candidate genes were associated with rwOS in patients with primary or metastatic tumors, showing an impressive 80% on-target identification rate (Figure 5); 9 in Chr 2 (Figure 5A), 1 in Chr X (Figure 5B), 10 in Chr 6 (Figure 5C), and LILRB4 in Chr 19 (Figure 5D). This finding also verified the high degree of common gene orthology between mouse and human genomes.

Candidate genes in human Chr 2 and Chr X were identified originally through mouse mammary tumor onset age. Chr 2 is the second-longest human chromosome, containing ~8% of the ~30,000 human genes (Human Genome Project), whereas Chr X is a sex-determining chromosome encoding ~800 genes (Uniprot, 2018). In the patients with primary, but not metastatic tumors, 4 out of 9 validated genes in human Chr 2 were favorably correlated with event-free days: namely GLI2, EPB41L5, CFAP221 and SCTR (Figure 5A and Table S3). Of these, GLI2 is critical for mammary gland development[41,42] and EPB41L5 is required for E-cadherin cell-cell adhesion,[43,44] whereas the roles of CFAP221 and the secretin receptor (SCTR) are not clear.[45–47] Expression of these genes may impede early events of tumor progression but may not alter the progression of advanced disease.

On the other hand, 5 genes were adversely associated with rwOS in both primary and metastatic diseases, namely NIFK, TMEM185B, DBI, STEAP3, and MARCO. NIFK is a partner of KI67 and a regulator of cell proliferation,[48] TMEM185B is a folate receptor-associated gene,[49] DBI is functional in lipid metabolism,[50] STEAP3 is a p53-inducible growth inhibitor[51,52] and facilitates transferrin-dependent iron uptake,[53,54] and MARCO is a scavenger receptor on adipocyte-specific macrophages.[55,56] Higher expression of these genes may render a survival advantage to the tumor cells, although the mechanisms are not yet defined.

In Chr X, expression of TSC22D3 was favorable for rwOS (Figure 5B). TSC22D3 is a transcription factor that is rapidly induced by the glucocorticoid receptor and interacts with NFKB/p52, NFKB/p65, RAF1, AP-1 and others to regulate the transcription of downstream genes.[57–61]

Ten candidate genes in human Chr 6 and LILRB4 in human Chr 19 were identified originally by analyzing mouse mammary tumor growth rate. Chr 6 contains 5.5–6% of human genes. Expression of FAM162B, GPRC6A, RFX6 were favorably associated with event-free days for both primary and metastatic diseases. VGLL2 and ROS1 were favorable predictors in metastatic, but not primary disease. GPRC6 mediates the activities of androgens.[62,63] RFX is associated with insulin activity and FAM162B with innervation of the colon and GI tract.[64] VGLL2 is a transcription factor regulating PPARγ activation,[65] whereas ROS1 is a proto-oncogene with tyrosine kinase activity.[66]

Adverse association with the outcome of primary or metastatic diseases was found in Chr 6 genes ASCC3, LILRB4A, DCBLD1, NUS1, CEP85L, and MCM9 (Figures 5C and 5D, Table S3). ASCC3 and MCM9 are associated with DNA repair,[67–70] CEP85L with centrosome integrity,[71,72] and NUS1 with angiogenesis.[73,74] DCBLD1 is an integrin receptor.[75,76] Another adverse predictor for both primary and metastatic diseases, LILRB4 on human Chr 19, is a negative regulator of inflammation and tumor immunity.[77–79] This set of genes is implicated in promoting tumor cell growth or impeding tumor immunity.

In summary, using the (BALBxDO) F1 NeuT model, we identified 28 candidate mouse genes across 3 QTL by their associations with tumor onset age or tumor growth rate. Human homologs are present for 26 of the 28 genes (Figure 6A). Of these 26 genes, 21 were significantly associated with event-free survival in the primary and/or metastatic cancer cohort. Expression of these candidate genes may prognosticate disease outcome in patients with breast cancer and potential targets of intervention.

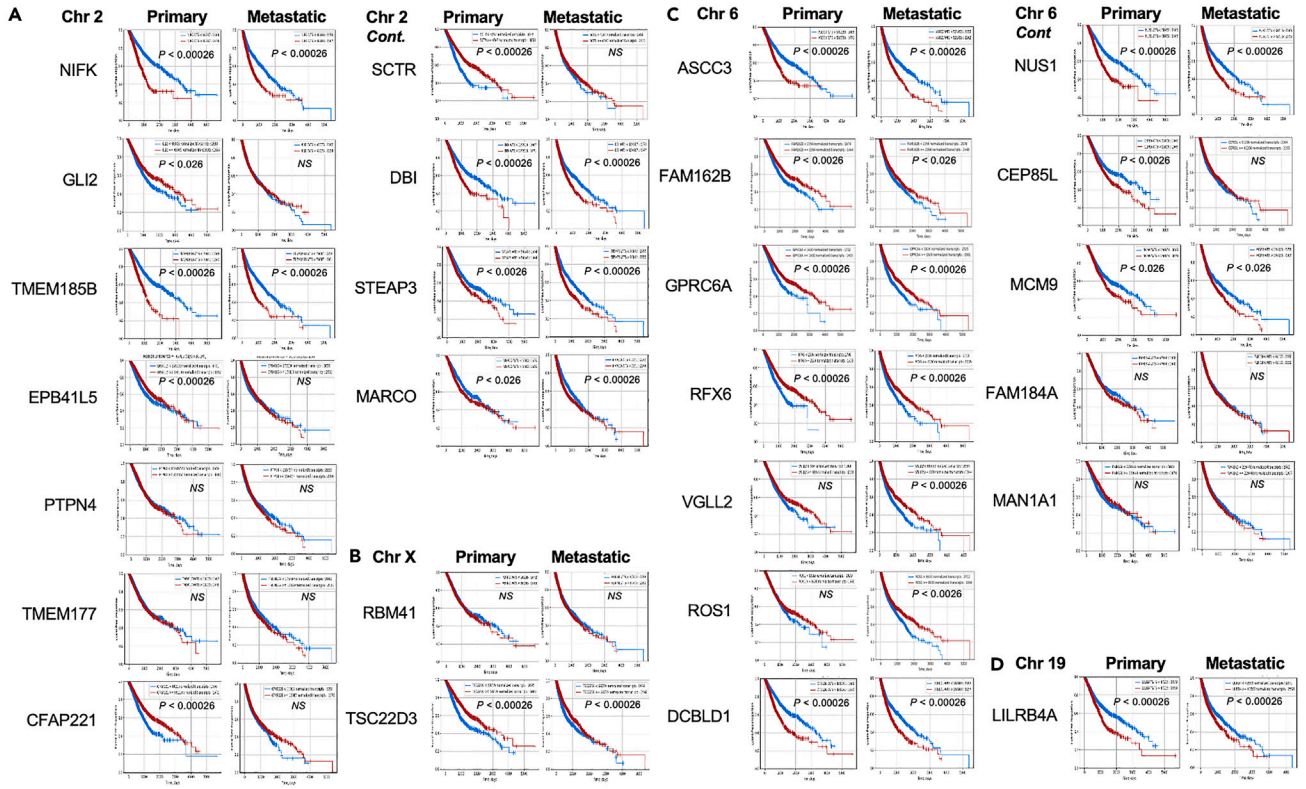

Figure 5. Kaplan-Meier survival analysis of women with primary or metastatic breast cancer

The Real World overall survival (rwOS) database was queried to determine the significance of identified genes in human breast cancer. Genes in human (A) Chr 2, (B) Chr X, (C) Chr 6 and (D) Chr 19 were queried in either primary or metastatic breast cancer patients. The logrank test was used to compare between groups and significance was determined as p values of < 0.05 after Bonferroni correction for multiple comparisons. Red lines indicate high gene expression, while blue lines indicate low gene expression.

Candidate gene pathway interactions

To determine whether candidate genes exert their effect individually or in concert, we entered the candidate gene list into IPA's Network Analysis tool.[80–82] Because IPA employs more resources than tumor onset age and growth rate, a more granular genetic interaction map can be constructed for direct testing. The resulting network plot (Figure 6B) shows that 12 of the 21 candidate genes share pathways. Four genes were central to the shared pathways: GLI2, TSC22D3, MARCO and LILRB4. All 4 genes influence the expression of immune cytokine genes IL6 and IL1B, whereas TNF expression is regulated by GLI2, TSC22D3, LILRB4, and GPRC6A. This finding suggests immune regulation of mammary tumor progression. Of particular interest is that TSC22D3 (Chr 6), a transcription factor, regulates the myeloid molecule LILRB4 (Chr 19) (Figure 6B, *blue boxes*).[83,84] Both genes were associated with tumor onset and growth rate in mice (Table S2) and significantly associated with survival in breast cancer patients (Figure 5).

Analysis of TSC22D3 and LILRB4 expression in BALB NeuT mammary tissues by scRNA-Seq revealed that although TSC22D3 was expressed in many cell types, LILRB4 was expressed primarily in myeloid/macrophages in normal, tumor or tumor adjacent mammary tissues (Figure S3). All known ligands of LILRB4 were also expressed within the mammary tissue microenvironment (Figure S3A), ALCAM (CD166) in epithelial cells in normal and tumor-adjacent tissue, APOE in macrophages, and FN1 (fibronectin) in stromal cells and tumor-associated macrophages. Expression of these ligands may enable continuous signaling via LILRB4 in myeloid cells.

When ligand expression in patients with primary or metastatic breast cancer was queried using CODEai, both APOE and FN1 expression were found to be adversely correlated with patient survival (Figure 6C), whereas ALCAM expression was favorable. Together, these results indicate that modulation of the LILRB4 signaling pathway is a plausible strategy for breast cancer intervention.

A Candidate Gene List

	Chr 2		Chr 6
✓	NIFK	✓	ASCC3
✓	GLI2	✓	FAM162B
✓	TMEM185B	✓	GPRC6A
✓	EPB4.1L5	✓	RFX6
	PTPN4	✓	VGLL2
	TMEM177	✓	ROS1
✓	CFAP221	✓	DCBLD1
✓	SCTR	✓	NUS1
✓	DBI	✓	CEP85L
✓	STEAP3	✓	MCM9
✓	MARCO		FAM184A
			MAN1A1
	Chr X		**Chr 19**
	RBM41	✓	LILRB4
✓	TSC22D3		

B Network Analysis

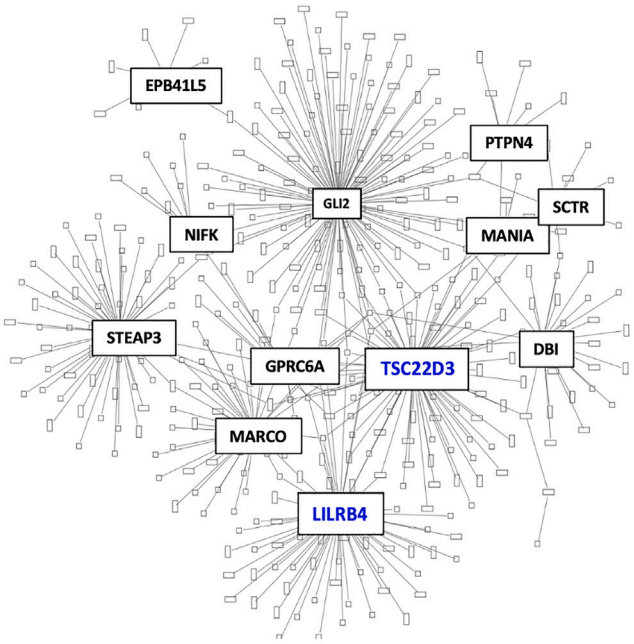

C LILRB4 ligands in breast cancer

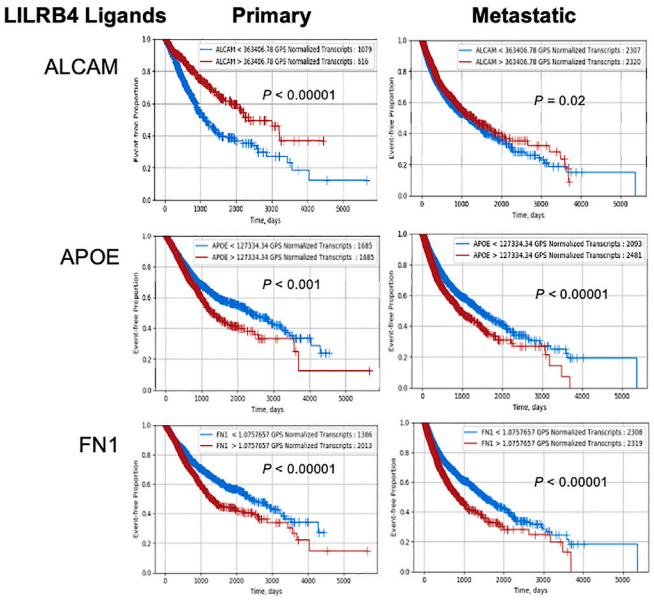

Figure 6. Network analysis of candidate genes

(A) Human homologues of candidate genes. A check-mark indicates genes which are significantly associated with primary or metastatic breast cancer outcome.

(B) IPA Network Analysis showing 12 genes with share pathways.

(C) Expression of the LILRB4 ligands ALCAM, APOE and FN1 were associated with event-free days in primary or metastatic breast cancer patients using Kaplan-Meier survival analysis. Red lines indicate gene expression above the average and blue lines indicate gene expression below the average. *p* values of < 0.05 were significant.

DISCUSSION

In this study we used both conventional and functional genomics approaches to investigate regulatory genes in breast cancer progression. Our results showed that loss of TIEG1 accelerated tumor progression and overpowered enhanced anti-tumor immunity, but that a stringent genome wide analysis process revealed humanly-relevant candidates of tumor onset and growth. TIEG1 has been associated with tumor suppressor activity, apart from its role in Treg induction.[32,85–87] Zhang et al.,[88] reported that TIEG1$^{-/-}$ mice showed accelerated papilloma development following chemical carcinogen exposure, consistent with deregulated epithelial cell cycle control in the absence of TIEG1. Although an interesting molecule, this functional dichotomy limits the utility of TIEG1 in cancer intervention.

We then established a HER2/Neu DO F1 discovery platform to associate genetic polymorphism with spontaneous tumor onset age and growth rate for the identification of actionable intervention targets. We performed genetic linkage analysis in female (BALBxDO) F1 NeuT mice, but it's worth noting that male (BALBxDO) F1 NeuT mice also displayed intriguing traits, such as more extensive and accelerated development of breast cancer with diminished salivary tumor formation, and preferential development of thoracic over inguinal mammary tumors. Although both thoracic and inguinal fat pads are white adipose tissue, the thoracic fat pads may provide a more permissive environment for tumor formation.[35,89,90] Further investigation of the difference(s) between the thoracic and inguinal fat pads in male mice may shed light in male breast cancer.

Interrogation of the Real-World Outcomes primary breast cancer dataset revealed 9 genes in Chr 2, 1 gene in Chr X, 10 genes in Chr 6, and LILRB4A in Chr 19 that were significantly associated with patient event-free days. Among the candidate genes, the simultaneous identification of LILRB4 and its transcription factor TSC22D3, is noteworthy. LILRB4 is emerging as a myeloid cell checkpoint molecule in solid tumors.[77] Compared to other cancer types, LILRB4 expression is particularly striking in breast cancer infiltrating CD45^{+} cells. Genetic knockout or mAb blockade of LILRB4 in mice delayed the outgrowth of transplanted solid tumors.[77] LILRB4 is a candidate intervention target for breast cancer prevention.

In addition to revealing a myeloid cell checkpoint receptor in the regulation of mammary tumor progression, several candidate genes are associated with normal mammary gland development (GLI2, EPB41L5) (Table S3), lipid metabolism (SCTR, DBI) and inflammation (TSC22D3, LILRB4, MARCO). Expression of SCTR which regulates lipolysis, was favorable for breast cancer outcome, whereas DBI which regulates long-chain fatty acids in peripheral tissues was adversely associated. Although adipocyte-specific inflammation is a key component of healthy adipose remodeling,[91] systemic inflammatory markers derived from both macrophages and adipocytes are associated with an increased risk of breast cancer.[92,93] Furthermore, MARCO, expressed by lipid-associated efferocytotic macrophages was adversely associated with disease outcomes. The interplay between lipid metabolism, inflammation and mammary gland development may influence HER2-induced breast cancer. Adiposity is a known risk factor for breast cancer development[94–96] with reduced levels of adiponectin and leptin associated with an increased risk of breast cancer.[93,97] In a recent study Oshi et al. determined that the level of adipogenesis in tumors was associated with overall survival in HER2^{+} and triple negative breast cancer patients and a change in macrophage infiltration.[98] Further analysis of these candidate molecules is warranted to better define their precise roles in breast cancer progression. Notably, the expression of ROS1 and VGLL2 was adversely associated with the survival of patients suffering from metastatic, but not primary breast cancer. ROS1 is a proto-oncogene with tyrosine kinase activity.[66] It may accelerate the progression of more advanced disease by synergizing with the downstream machineries of multiple oncogenes. Although this is a speculative notion, it may be prudent to evaluate ROS1 inhibitors in clinical trials with this new perspective. Unfortunately, the mechanism of VGLL2 in cancer progression is not well defined, but higher expression of this gene is also associated with poorer survival from metastatic breast cancer.

In this study, the driving founder strain, PWK, was verified by crossing them with BALB NeuT, i.e., (BALBxPWK) F1 NeuT mice. Alternatively, verification could be considered in F1 mice mated with collaborative cross (CC) strains[20,21] that share the QTL haplotypes. Either approach provides necessary validation to the gene discovery process.

Regarding the logistics of DO QTL study, (BALBxDO) F1 NeuT mice were generated by breeding BALB NeuT male mice with DO female mice. The average litter size was 5 mice. Approximately half of the females were NeuT^{+} as determined by PCR analysis, therefore, an average of 1–2 female mice per litter were

entered into the study, with minimal genetic relatedness among the test mice. In addition, breeder DO females were used only once in the same experiment to ensure genetic heterogeneity. The genetic unrelatedness of test mice was demonstrated by R/QTL kinship analysis.

Winter et al. reported a DO F1 genetic risk gene study in TRAMP mice.[99] TRAMP mice express Simian virus 40 large T (SV40 LT) antigen in prostatic epithelium under the rat probasin promoter so that male mice develop prostate cancer. Prostate cancer in TRAMP mice has mixed phenotypes. Still, (B6xDO) F1 TRAMP mice showed more variable tumor progression when compared to those in a syngeneic B6 background. A QTL in chromosome 8 was associated with more aggressive disease, but candidate genes were not identified based on founder QTL effect. Rather, RNA expression levels were analyzed against disease aggressiveness. One limitation of the TRAMP model is the use of SV40 LT as the cancer driver. Because SV40 is not a natural driver in human prostate cancer, genes associated with SV40 LT oncogenesis may not reflect the regulatory mechanism(s) in the human prostate. For impactful gene discovery, it is important to interrogate model systems induced by actual human oncogenes or carcinogens so that the captured cancer risk genes are relevant to human diseases.

Yang et al. interrogated DO mice exposed to dimethylbenz[a]anthracene (DMBA) to identify four genes associated with the development of pancreatic cancer: Epha4 (an ephrin receptor, important in development), Gpc5 (Glypican 5, involved in cell growth and division), Kcnj6 (potassium channel gene) and Arid1b (a component of the SWI/SNF chromatin remodeling complex).[100] A single SNP in Gpc5, which was associated with reduced gene expression, demonstrated the strongest correlation with pancreatic cancer progression and a putative suppressor of disease progression. Consistent with our findings, the authors identified genes involved in development, cell growth and chromosomal integrity.

To the best of our knowledge, ours is the first report that revealed heritable risk genes associated with HER2 or any oncogene-induced tumors. That human cancer risk genes were predicted from the candidate mouse genes validates the process and discovery power of the DO F1 platform. These genes provide avenues for disease prediction, treatment, or prevention.

Limitations of the study

In this study, we interrogated DO F1 mice as opposed to DO mice. DO mice carry 2 mosaic chromosomes and 36 possible diplotypes, whereas DO F1 mice carry a single mosaic chromosome from the DO parent, resulting in 8 possible diplotypes. Thus when the haplotype from a DO founder strain drives the phenotype as we observed with PWK and CAST, the contributing genes are dominant because only one copy of the gene is present. Recessive genes are much less likely to be discovered in this platform and this is a limitation. The reduced degrees of freedom also reduced the sample size required for genetic linkage analysis and enabled us to obtain meaningful results with ~100 mice. We recognize, however, that adding more mice to the study can improve clarity in identifying candidate genes. In this study, we focused on genes which harbored SNP in the coding regions; however, many SNP are found in non-coding regions and thus excluded by the current analysis. Future work will investigate SNP in non-coding region(s) utilizing ATAC-seq and RNA-seq on the same samples. scRNA-Seq is a powerful tool in identifying cell populations expressing gene(s) of interest. This approach captures gene expression at a selected timepoint and this could be a limitation. The scRNA libraries we reported here do not fully capture the dynamics of gene expression during tumor development.

STAR★METHODS

Detailed methods are provided in the online version of this paper and include the following:

- KEY RESOURCES TABLE
- RESOURCE AVAILABILITY
  - Lead contact
  - Materials availability
  - Data and code availability
- EXPERIMENTAL MODEL AND SUBJECT DETAILS
  - B6 HER2 Tg mice
  - B6 TIEG1$^{-/-}$HER2 Tg mice
  - BALB NeuT mice

SUPPLEMENTAL INFORMATION

Supplemental information can be found online at https://doi.org/10.1016/j.isci.2023.106320.

ACKNOWLEDGMENTS

The authors thank Dr. Venuprassad Poojary for his support in the TIEG1 research, Dr. Steve Ethier for his guidance on genomics analysis, and Dr. Jeff Frelinger for his advice on genetic linkage analysis of the Diversity Outbred mice. We thank the staff of the Animal Model and Therapeutics Evaluation Core (AMTEC) for their expert technical assistance. Flow cytometry assistance was rendered by the Microscopy, Imaging and Cytometry Resources (MICR) core. We thank Drs. Roger Pique and Adnan Alazzizi of the Genomics Core for their support of the Single Cell RNA analysis. This work was funded by CA76340 and The Herrick Foundation (WZW), Karmanos Tumor Biology and Microenvironment Program (JBJ) and CCSG P30 CA022453 (GB).

AUTHOR CONTRIBUTIONS

Study design, data generation, data analysis: J.B.J., K-C.W., J.R., A.C., K.W., N.V., J.M., C.Y., V.P., and W-Z.W. Statistical support: S.K. Manuscript preparation: J.B.J. and W-Z.W. Contribution of knowledge, improvement of manuscript: all authors.

DECLARATION OF INTERESTS

The authors declare no competing interests.

Received: August 29, 2022
Revised: January 16, 2023
Accepted: February 26, 2023
Published: March 2, 2023

REFERENCES

1. Manolio, T.A., Collins, F.S., Cox, N.J., Goldstein, D.B., Hindorff, L.A., Hunter, D.J., McCarthy, M.I., Ramos, E.M., Cardon, L.R., Chakravarti, A., et al. (2009). Finding the missing heritability of complex diseases. Nature *461*, 747–753. https://doi.org/10.1038/nature08494.

2. Sud, A., Kinnersley, B., and Houlston, R.S. (2017). Genome-wide association studies of cancer: current insights and future perspectives. Nat. Rev. Cancer *17*, 692–704. https://doi.org/10.1038/nrc.2017.82.

3. Fanfani, V., Citi, L., Harris, A.L., Pezzella, F., and Stracquadanio, G. (2021). The Landscape of the heritable cancer genome. Cancer Res. *81*, 2588–2599. https://doi.org/10.1158/0008-5472.CAN-20-3348.

4. Cao, Z., Sun, X., Icli, B., Wara, A.K., and Feinberg, M.W. (2010). Role of Kruppel-like factors in leukocyte development, function, and disease. Blood *116*, 4404–4414. https://doi.org/10.1182/blood-2010-05-285353.

5. Subramaniam, M., Harris, S.A., Oursler, M.J., Rasmussen, K., Riggs, B.L., and Spelsberg, T.C. (1995). Identification of a novel TGF-beta-regulated gene encoding a putative zinc finger protein in human osteoblasts. Nucleic Acids Res. *23*, 4907–4912. https://doi.org/10.1093/nar/23.23.4907.

6. Theivanthiran, B., Kathania, M., Zeng, M., Anguiano, E., Basrur, V., Vandergriff, T., Pascual, V., Wei, W.Z., Massoumi, R., and Venuprasad, K. (2015). The E3 ubiquitin ligase Itch inhibits p38alpha signaling and skin inflammation through the ubiquitylation of Tab1. Sci. Signal. *8*, ra22. https://doi.org/10.1126/scisignal.2005903.

7. Venuprasad, K., Huang, H., Harada, Y., Elly, C., Subramaniam, M., Spelsberg, T., Su, J., and Liu, Y.C. (2008). The E3 ubiquitin ligase Itch regulates expression of transcription factor Foxp3 and airway inflammation by enhancing the function of transcription factor TIEG1. Nat. Immunol. *9*, 245–253. https://doi.org/10.1038/ni1564.

8. Cao, Z., Wara, A.K., Icli, B., Sun, X., Packard, R.R.S., Esen, F., Stapleton, C.J., Subramaniam, M., Kretschmer, K., Apostolou, I., et al. (2009). Kruppel-like factor KLF10 targets transforming growth factor-beta1 to regulate CD4(+)CD25(-) T cells and T regulatory cells. J. Biol. Chem. *284*, 24914–24924. https://doi.org/10.1074/jbc.M109.000059.

9. Xiong, Y., Khanna, S., Grzenda, A.L., Sarmento, O.F., Svingen, P.A., Lomberk, G.A., Urrutia, R.A., and Faubion, W.A., Jr. (2012). Polycomb antagonizes p300/CREB-binding protein-associated factor to silence FOXP3 in a Kruppel-like factor-dependent manner. J. Biol. Chem. *287*, 34372–34385. https://doi.org/10.1074/jbc.M111.325332.

10. Peng, D.J., Zeng, M., Muromoto, R., Matsuda, T., Shimoda, K., Subramaniam, M., Spelsberg, T.C., Wei, W.Z., and Venuprasad, K. (2011). Noncanonical K27-linked polyubiquitination of TIEG1 regulates Foxp3 expression and tumor growth. J. Immunol. *186*, 5638–5647. https://doi.org/10.4049/jimmunol.1003801.

11. Jacob, J.B., Kong, Y.c.M., Meroueh, C., Snower, D.P., David, C.S., Ho, Y.S., and Wei, W.Z. (2007). Control of Her-2 tumor immunity and thyroid autoimmunity by MHC and regulatory T cells. Cancer Res. *67*, 7020–7027. https://doi.org/10.1158/0008-5472.CAN-06-4755.

12. Wei, W.Z., Jacob, J.B., Zielinski, J.F., Flynn, J.C., Shim, K.D., Alsharabi, G., Giraldo, A.A., and Kong, Y.c.M. (2005). Concurrent induction of antitumor immunity and autoimmune thyroiditis in CD4+ CD25+ regulatory T cell-depleted mice. Cancer Res. *65*, 8471–8478. https://doi.org/10.1158/0008-5472.CAN-05-0934.

13. Muller, W.J., Sinn, E., Pattengale, P.K., Wallace, R., and Leder, P. (1988). Single-step induction of mammary adenocarcinoma in transgenic mice bearing the activated c-neu oncogene. Cell *54*, 105–115. https://doi.org/10.1016/0092-8674(88)90184-5.

14. Saul, M.C., Philip, V.M., Reinholdt, L.G.; Center for Systems Neurogenetics of Addiction, and Chesler, E.J. (2019). High-diversity mouse populations for complex traits. Trends Genet. *35*, 501–514. https://doi.org/10.1016/j.tig.2019.04.003.

15. Huda, M.N., VerHague, M., Albright, J., Smallwood, T., Bell, T.A., Que, E., Miller, D.R., Roshanravan, B., Allayee, H., Manuel de Villena, F.P., and Bennett, B.J. (2020). Dissecting the genetic Architecture of Cystatin C in diversity outbred mice. G3 (Bethesda) *10*, 2529–2541. https://doi.org/10.1534/g3.120.401275.

16. Shorter, J.R., Huang, W., Beak, J.Y., Hua, K., Gatti, D.M., de Villena, F.P.M., Pomp, D., and Jensen, B.C. (2018). Quantitative trait mapping in Diversity Outbred mice identifies two genomic regions associated with heart size. Mamm. Genome *29*, 80–89. https://doi.org/10.1007/s00335-017-9730-7.

17. Harrill, A.H., Borghoff, S., Zorrilla, L., Blystone, C., Kissling, G.E., Malarkey, D., Shockley, K., Travlos, G., and DeVito, M.J. (2018). In NTP Research Report on Baseline Characteristics of Diversity Outbred (J:DO) Mice Relevant to Toxicology Studies: Research Report 6.

18. Kurtz, S.L., Gardina, P.J., Myers, T.G., Rydén, P., and Elkins, K.L. (2020). Whole genome profiling refines a panel of correlates to predict vaccine efficacy against. Tuberculosis *120*, 101895. https://doi.org/10.1016/j.tube.2019.101895.

19. Kurtz, S.L., Rossi, A.P., Beamer, G.L., Gatti, D.M., Kramnik, I., and Elkins, K.L. (2020). The diversity outbred mouse population is an improved animal model of vaccination against Tuberculosis that reflects heterogeneity of Protection. mSphere *5*. https://doi.org/10.1128/mSphere.00097-20.

20. Churchill, G.A., Airey, D.C., Allayee, H., Angel, J.M., Attie, A.D., Beatty, J., Beavis, W.D., Belknap, J.K., Bennett, B., Berrettini, W., et al. (2004). The Collaborative Cross, a community resource for the genetic analysis of complex traits. Nat. Genet. *36*, 1133–1137. https://doi.org/10.1038/ng1104-1133.

21. Threadgill, D.W., Hunter, K.W., and Williams, R.W. (2002). Genetic dissection of complex and quantitative traits: from fantasy to reality via a community effort. Mamm. Genome *13*, 175–178. https://doi.org/10.1007/s00335-001-4001-Y.

22. Wei, W.Z., Gibson, H.M., Jacob, J.B., Frelinger, J.A., Berzofsky, J.A., Maeng, H., Dyson, G., Reyes, J.D., Pilon-Thomas, S., Ratner, S., and Wei, K.C. (2020). Diversity outbred mice reveal the quantitative trait locus and regulatory cells of HER2 immunity. J. Immunol. *205*, 1554–1563. https://doi.org/10.4049/jimmunol.2000466.

23. Bargmann, C.I., Hung, M.C., and Weinberg, R.A. (1986). Multiple independent activations of the neu oncogene by a point mutation altering the transmembrane domain of p185. Cell *45*, 649–657. https://doi.org/10.1016/0092-8674(86)90779-8.

24. Li, J., Zheng, H., Bates, P.J., Malik, T., Li, X.F., Trent, J.O., and Ng, C.K. (2014). Aptamer imaging with Cu-64 labeled AS1411: preliminary assessment in lung cancer. Nucl. Med. Biol. *41*, 179–185. https://doi.org/10.1016/j.nucmedbio.2013.10.008.

25. Dorrity, M.W., Saunders, L.M., Queitsch, C., Fields, S., and Trapnell, C. (2020). Dimensionality reduction by UMAP to visualize physical and genetic interactions. Nat. Commun. *11*, 1537. https://doi.org/10.1038/s41467-020-15351-4.

26. Hao, Y., Hao, S., Andersen-Nissen, E., Mauck, W.M., 3rd, Zheng, S., Butler, A., Lee, M.J., Wilk, A.J., Darby, C., Zager, M., et al. (2021). Integrated analysis of multimodal single-cell data. Cell *184*, 3573–3587.e29. https://doi.org/10.1016/j.cell.2021.04.048.

27. Piechocki, M.P., Ho, Y.S., Pilon, S., and Wei, W.Z. (2003). Human ErbB-2 (Her-2) transgenic mice: a model system for testing Her-2 based vaccines. J. Immunol. *171*, 5787–5794. https://doi.org/10.4049/jimmunol.171.11.5787.

28. Radkevich-Brown, O., Jacob, J., Kershaw, M., and Wei, W.Z. (2009). Genetic regulation of the response to Her-2 DNA vaccination in human Her-2 transgenic mice. Cancer Res. *69*, 212–218. https://doi.org/10.1158/0008-5472.CAN-08-3092.

29. Jacob, J.B., Quaglino, E., Radkevich-Brown, O., Jones, R.F., Piechocki, M.P., Reyes, J.D., Weise, A., Amici, A., and Wei, W.Z. (2010). Combining human and rat sequences in her-2 DNA vaccines blunts immune tolerance and drives antitumor immunity. Cancer Res. *70*, 119–128. https://doi.org/10.1158/0008-5472.CAN-09-2554.

30. Tachibana, I., Imoto, M., Adjei, P.N., Gores, G.J., Subramaniam, M., Spelsberg, T.C., and Urrutia, R. (1997). Overexpression of the TGFbeta-regulated zinc finger encoding gene, TIEG, induces apoptosis in pancreatic epithelial cells. J. Clin. Invest. *99*, 2365–2374. https://doi.org/10.1172/JCI119418.

31. Tau, K.R., Hefferan, T.E., Waters, K.M., Robinson, J.A., Subramaniam, M., Riggs, B.L., and Spelsberg, T.C. (1998). Estrogen regulation of a transforming growth factor-beta inducible early gene that inhibits deoxyribonucleic acid synthesis in human osteoblasts. Endocrinology *139*, 1346–1353. https://doi.org/10.1210/endo.139.3.5830.

32. Jin, W., Chen, B.B., Li, J.Y., Zhu, H., Huang, M., Gu, S.M., Wang, Q.Q., Chen, J.Y., Yu, S., Wu, J., and Shao, Z.M. (2012). TIEG1 inhibits breast cancer invasion and metastasis by inhibition of epidermal growth factor receptor (EGFR) transcription and the EGFR signaling pathway. Mol. Cell Biol. *32*, 50–63. https://doi.org/10.1128/MCB.06152-11.

33. Churchill, G.A., Gatti, D.M., Munger, S.C., and Svenson, K.L. (2012). The Diversity Outbred mouse population. Mamm. Genome *23*, 713–718. https://doi.org/10.1007/s00335-012-9414-2.

34. Gatti, D.M., Svenson, K.L., Shabalin, A., Wu, L.Y., Valdar, W., Simecek, P., Goodwin, N., Cheng, R., Pomp, D., Palmer, A., et al. (2014). Quantitative trait locus mapping methods for diversity outbred mice. G3 (Bethesda) *4*, 1623–1633. https://doi.org/10.1534/g3.114.013748.

35. Burl, R.B., Ramseyer, V.D., Rondini, E.A., Pique-Regi, R., Lee, Y.H., and Granneman, J.G. (2018). Deconstructing adipogenesis induced by beta3-Adrenergic receptor activation with single-cell expression profiling. Cell Metab. *28*, 300–309.e4. https://doi.org/10.1016/j.cmet.2018.05.025.

36. Broman, K.W., Gatti, D.M., Simecek, P., Furlotte, N.A., Prins, P., Sen, Ś., Yandell, B.S., and Churchill, G.A. (2019). R/qtl2: software for mapping quantitative trait Loci with high-dimensional data and Multiparent

populations. Genetics *211*, 495–502. https://doi.org/10.1534/genetics.118.301595.

37. Charlebois, D.A., and Balázsi, G. (2019). Modeling cell population dynamics. Silico Biol. *13*, 21–39. https://doi.org/10.3233/ISB-180470.

38. Loree, J.M., Wang, Y., Syed, M.A., Sorokin, A.V., Coker, O., Xiu, J., Weinberg, B.A., Vanderwalde, A.M., Tesfaye, A., Raymond, V.M., et al. (2021). Clinical and functional Characterization of Atypical KRAS/NRAS mutations in metastatic Colorectal cancer. Clin. Cancer Res. *27*, 4587–4598. https://doi.org/10.1158/1078-0432.CCR-21-0180.

39. Abraham, J.P., Magee, D., Cremolini, C., Antoniotti, C., Halbert, D.D., Xiu, J., Stafford, P., Berry, D.A., Oberley, M.J., Shields, A.F., et al. (2021). Clinical validation of a Machine-learning-derived Signature predictive of outcomes from first-line Oxaliplatin-based Chemotherapy in advanced Colorectal cancer. Clin. Cancer Res. *27*, 1174–1183. https://doi.org/10.1158/1078-0432.CCR-20-3286.

40. Von Hoff, D.D., Stephenson, J.J., Jr., Rosen, P., Loesch, D.M., Borad, M.J., Anthony, S., Jameson, G., Brown, S., Cantafio, N., Richards, D.A., et al. (2010). Pilot study using molecular profiling of patients' tumors to find potential targets and select treatments for their refractory cancers. J. Clin. Oncol. *28*, 4877–4883. https://doi.org/10.1200/JCO.2009.26.5983.

41. Ruppert, J.M., Kinzler, K.W., Wong, A.J., Bigner, S.H., Kao, F.T., Law, M.L., Seuanez, H.N., O'Brien, S.J., and Vogelstein, B. (1988). The GLI-Kruppel family of human genes. Mol. Cell Biol. *8*, 3104–3113. https://doi.org/10.1128/mcb.8.8.3104.

42. Lewis, M.T., Ross, S., Strickland, P.A., Sugnet, C.W., Jimenez, E., Hui, C., and Daniel, C.W. (2001). The Gli2 transcription factor is required for normal mouse mammary gland development. Dev. Biol. *238*, 133–144. https://doi.org/10.1006/dbio.2001.0410.

43. Gosens, I., Sessa, A., den Hollander, A.I., Letteboer, S.J.F., Belloni, V., Arends, M.L., Le Bivic, A., Cremers, F.P.M., Broccoli, V., and Roepman, R. (2007). FERM protein EPB41L5 is a novel member of the mammalian CRB-MPP5 polarity complex. Exp. Cell Res. *313*, 3959–3970. https://doi.org/10.1016/j.yexcr.2007.08.025.

44. Lee, J.D., Silva-Gagliardi, N.F., Tepass, U., McGlade, C.J., and Anderson, K.V. (2007). The FERM protein Epb4.1l5 is required for organization of the neural plate and for the epithelial-mesenchymal transition at the primitive streak of the mouse embryo. Development *134*, 2007–2016. https://doi.org/10.1242/dev.000885.

45. Lee, L., Campagna, D.R., Pinkus, J.L., Mulhern, H., Wyatt, T.A., Sisson, J.H., Pavlik, J.A., Pinkus, G.S., and Fleming, M.D. (2008). Primary ciliary dyskinesia in mice lacking the novel ciliary protein Pcdp1. Mol. Cell Biol. *28*, 949–957. https://doi.org/10.1128/MCB.00354-07.

46. Sekar, R., and Chow, B.K.C. (2014). Secretin receptor-knockout mice are resistant to high-fat diet-induced obesity and exhibit impaired intestinal lipid absorption. FASEB J *28*, 3494–3505. https://doi.org/10.1096/fj.13-247536.

47. Chu, J.Y.S., Chung, S.C.K., Lam, A.K.M., Tam, S., Chung, S.K., and Chow, B.K.C. (2007). Phenotypes developed in secretin receptor-null mice indicated a role for secretin in regulating renal water reabsorption. Mol. Cell Biol. *27*, 2499–2511. https://doi.org/10.1128/MCB.01088-06.

48. Takagi, M., Sueishi, M., Saiwaki, T., Kametaka, A., and Yoneda, Y. (2001). A novel nucleolar protein, NIFK, interacts with the forkhead associated domain of Ki-67 antigen in mitosis. J. Biol. Chem. *276*, 25386–25391. https://doi.org/10.1074/jbc.M102227200.

49. Shaw, M.A., Chiurazzi, P., Romain, D.R., Neri, G., and Gécz, J. (2002). A novel gene, FAM11A, associated with the FRAXF CpG island is transcriptionally silent in FRAXF full mutation. Eur. J. Hum. Genet. *10*, 767–772. https://doi.org/10.1038/sj.ejhg.5200881.

50. Bravo-San Pedro, J.M., Sica, V., Martins, I., Pol, J., Loos, F., Maiuri, M.C., Durand, S., Bossut, N., Aprahamian, F., Anagnostopoulos, G., et al. (2019). Acyl-CoA-binding protein is a Lipogenic factor that Triggers Food Intake and obesity. Cell Metab. *30*, 754–767.e9. https://doi.org/10.1016/j.cmet.2019.07.010.

51. Lespagnol, A., Duflaut, D., Beekman, C., Blanc, L., Fiucci, G., Marine, J.C., Vidal, M., Amson, R., and Telerman, A. (2008). Exosome secretion, including the DNA damage-induced p53-dependent secretory pathway, is severely compromised in TSAP6/Steap3-null mice. Cell Death Differ. *15*, 1723–1733. https://doi.org/10.1038/cdd.2008.104.

52. Wang, L.L., Luo, J., He, Z.H., Liu, Y.Q., Li, H.G., Xie, D., and Cai, M.Y. (2021). STEAP3 promotes cancer cell proliferation by facilitating nuclear trafficking of EGFR to enhance RAC1-ERK-STAT3 signaling in hepatocellular carcinoma. Cell Death Dis. *12*, 1052. https://doi.org/10.1038/s41419-021-04329-9.

53. Ohgami, R.S., Campagna, D.R., Greer, E.L., Antiochos, B., McDonald, A., Chen, J., Sharp, J.J., Fujiwara, Y., Barker, J.E., and Fleming, M.D. (2005). Identification of a ferrireductase required for efficient transferrin-dependent iron uptake in erythroid cells. Nat. Genet. *37*, 1264–1269. https://doi.org/10.1038/ng1658.

54. Ohgami, R.S., Campagna, D.R., McDonald, A., and Fleming, M.D. (2006). The Steap proteins are metalloreductases. Blood *108*, 1388–1394. https://doi.org/10.1182/blood-2006-02-003681.

55. Arredouani, M.S., and Kobzik, L. (2004). The structure and function of marco, a macrophage class a scavenger receptor. Cell Mol Biol (Noisy-le-grand) *50*, 657–665.

56. Georgoudaki, A.M., Prokopec, K.E., Boura, V.F., Hellqvist, E., Sohn, S., Östling, J., Dahan, R., Harris, R.A., Rantalainen, M., Klevebring, D., et al. (2016). Reprogramming tumor-associated macrophages by Antibody targeting inhibits cancer progression and metastasis. Cell Rep. *15*, 2000–2011. https://doi.org/10.1016/j.celrep.2016.04.084.

57. Mittelstadt, P.R., and Ashwell, J.D. (2001). Inhibition of AP-1 by the glucocorticoid-inducible protein GILZ. J. Biol. Chem. *276*, 29603–29610. https://doi.org/10.1074/jbc.M101522200.

58. Ayroldi, E., Migliorati, G., Bruscoli, S., Marchetti, C., Zollo, O., Cannarile, L., D'Adamio, F., and Riccardi, C. (2001). Modulation of T-cell activation by the glucocorticoid-induced leucine zipper factor via inhibition of nuclear factor kappaB. Blood *98*, 743–753. https://doi.org/10.1182/blood.v98.3.743.

59. Ayroldi, E., Zollo, O., Macchiarulo, A., Di Marco, B., Marchetti, C., and Riccardi, C. (2002). Glucocorticoid-induced leucine zipper inhibits the Raf-extracellular signal-regulated kinase pathway by binding to Raf-1. Mol. Cell Biol. *22*, 7929–7941. https://doi.org/10.1128/MCB.22.22.7929-7941.2002.

60. Bereshchenko, O., Migliorati, G., Bruscoli, S., and Riccardi, C. (2019). Glucocorticoid-induced leucine zipper: anovel anti-inflammatory molecule. Front. Pharmacol. *10*, 308. https://doi.org/10.3389/fphar.2019.00308.

61. D'Adamio, F., Zollo, O., Moraca, R., Ayroldi, E., Bruscoli, S., Bartoli, A., Cannarile, L., Migliorati, G., and Riccardi, C. (1997). A new dexamethasone-induced gene of the leucine zipper family protects T lymphocytes from TCR/CD3-activated cell death. Immunity *7*, 803–812. https://doi.org/10.1016/s1074-7613(00)80398-2.

62. Ye, R., Pi, M., Nooh, M.M., Bahout, S.W., and Quarles, L.D. (2019). Human GPRC6A mediates Testosterone-induced Mitogen-activated protein kinases and mTORC1 signaling in prostate cancer cells. Mol. Pharmacol. *95*, 563–572. https://doi.org/10.1124/mol.118.115014.

63. Jørgensen, S., Have, C.T., Underwood, C.R., Johansen, L.D., Wellendorph, P., Gjesing, A.P., Jørgensen, C.V., Quan, S., Rui, G., Inoue, A., et al. (2017). Genetic variations in the human G protein-coupled receptor class C, group 6, member A (GPRC6A) control cell surface expression and function. J. Biol. Chem. *292*, 1524–1534. https://doi.org/10.1074/jbc.M116.756577.

64. Mungall, A.J., Palmer, S.A., Sims, S.K., Edwards, C.A., Ashurst, J.L., Wilming, L., Jones, M.C., Horton, R., Hunt, S.E., Scott, C.E., et al. (2003). The DNA sequence and analysis of human chromosome 6. Nature *425*, 805–811. https://doi.org/10.1038/nature02055.

65. Mesrouze, Y., Aguilar, G., Bokhovchuk, F., Martin, T., Delaunay, C., Villard, F., Meyerhofer, M., Zimmermann, C., Fontana, P., Wille, R., et al. (2020). A new perspective

on the interaction between the Vg/VGLL1-3 proteins and the TEAD transcription factors. Sci. Rep. *10*, 17442. https://doi.org/10.1038/s41598-020-74584-x.

66. Matsushime, H., Wang, L.H., and Shibuya, M. (1986). Human c-ros-1 gene homologous to the v-ros sequence of UR2 sarcoma virus encodes for a transmembrane receptorlike molecule. Mol. Cell Biol. *6*, 3000–3004. https://doi.org/10.1128/mcb.6.8.3000-3004.1986.

67. Soll, J.M., Brickner, J.R., Mudge, M.C., and Mosammaparast, N. (2018). RNA ligase-like domain in activating signal cointegrator 1 complex subunit 1 (ASCC1) regulates ASCC complex function during alkylation damage. J. Biol. Chem. *293*, 13524–13533. https://doi.org/10.1074/jbc.RA117.000114.

68. Jung, D.J., Sung, H.S., Goo, Y.W., Lee, H.M., Park, O.K., Jung, S.Y., Lim, J., Kim, H.J., Lee, S.K., Kim, T.S., et al. (2002). Novel transcription coactivator complex containing activating signal cointegrator 1. Mol. Cell Biol. *22*, 5203–5211. https://doi.org/10.1128/MCB.22.14.5203-5211.2002.

69. Bailis, J.M., and Forsburg, S.L. (2004). MCM proteins: DNA damage, mutagenesis and repair. Curr. Opin. Genet. Dev. *14*, 17–21. https://doi.org/10.1016/j.gde.2003.11.002.

70. Lutzmann, M., Maiorano, D., and Méchali, M. (2005). Identification of full genes and proteins of MCM9, a novel, vertebrate-specific member of the MCM2-8 protein family. Gene *362*, 51–56. https://doi.org/10.1016/j.gene.2005.07.031.

71. Jakobsen, L., Vanselow, K., Skogs, M., Toyoda, Y., Lundberg, E., Poser, I., Falkenby, L.G., Bennetzen, M., Westendorf, J., Nigg, E.A., et al. (2011). Novel asymmetrically localizing components of human centrosomes identified by complementary proteomics methods. EMBO J. *30*, 1520–1535. https://doi.org/10.1038/emboj.2011.63.

72. Tsai, M.H., Muir, A.M., Wang, W.J., Kang, Y.N., Yang, K.C., Chao, N.H., Wu, M.F., Chang, Y.C., Porter, B.E., Jansen, L.A., et al. (2020). Pathogenic Variants in CEP85L Cause sporadic and Familial Posterior Predominant Lissencephaly. Neuron *106*, 237–245.e8. https://doi.org/10.1016/j.neuron.2020.01.027.

73. Wu, D., Zhao, B., Qi, X., Peng, F., Fu, H., Chi, X., Miao, Q.R., and Shao, S. (2018). Nogo-B receptor promotes epithelial-mesenchymal transition in non-small cell lung cancer cells through the Ras/ERK/Snail1 pathway. Cancer Lett. *418*, 135–146. https://doi.org/10.1016/j.canlet.2018.01.030.

74. Zhang, Y., Wang, L., Zhang, Y., Wang, M., Sun, Q., Xia, F., Wang, R., and Liu, L. (2017). Nogo-B promotes angiogenesis in proliferative Diabetic Retinopathy via VEGF/PI3K/Akt pathway in an Autocrine manner. Cell. Physiol. Biochem. *43*, 1742–1754. https://doi.org/10.1159/000484061.

75. Schmoker, A.M., Ebert, A.M., and Ballif, B.A. (2019). The DCBLD receptor family: emerging signaling roles in development, homeostasis and disease. Biochem. J. *476*, 931–950. https://doi.org/10.1042/BCJ20190022.

76. Schmoker, A.M., Weinert, J.L., Kellett, K.J., Johnson, H.E., Joy, R.M., Weir, M.E., Ebert, A.M., and Ballif, B.A. (2017). Dynamic multi-site phosphorylation by Fyn and Abl drives the interaction between CRKL and the novel scaffolding receptors DCBLD1 and DCBLD2. Biochem. J. *474*, 3963–3984. https://doi.org/10.1042/BCJ20170615.

77. Sharma, N., Atolagbe, O.T., Ge, Z., and Allison, J.P. (2021). LILRB4 suppresses immunity in solid tumors and is a potential target for immunotherapy. J. Exp. Med. *218*, e20201811. https://doi.org/10.1084/jem.20201811.

78. Cella, M., Döhring, C., Samaridis, J., Dessing, M., Brockhaus, M., Lanzavecchia, A., and Colonna, M. (1997). A novel inhibitory receptor (ILT3) expressed on monocytes, macrophages, and dendritic cells involved in antigen processing. J. Exp. Med. *185*, 1743–1751. https://doi.org/10.1084/jem.185.10.1743.

79. Deng, M., Gui, X., Kim, J., Xie, L., Chen, W., Li, Z., He, L., Chen, Y., Chen, H., Luo, W., et al. (2018). LILRB4 signalling in leukaemia cells mediates T cell suppression and tumour infiltration. Nature *562*, 605–609. https://doi.org/10.1038/s41586-018-0615-z.

80. Talman, V., Teppo, J., Pöhö, P., Movahedi, P., Vaikkinen, A., Karhu, S.T., Trošt, K., Suvitaival, T., Heikkonen, J., Pahikkala, T., et al. (2018). Molecular Atlas of Postnatal mouse heart development. J. Am. Heart Assoc. *7*, e010378. https://doi.org/10.1161/JAHA.118.010378.

81. Ayers, J., Milner, R.J., Cortés-Hinojosa, G., Riva, A., Bechtel, S., Sahay, B., Cascio, M., Lejeune, A., Shiomitsu, K., Souza, C., et al. (2021). Novel application of single-cell next-generation sequencing for determination of intratumoral heterogeneity of canine osteosarcoma cell lines. J. Vet. Diagn. Invest. *33*, 261–278. https://doi.org/10.1177/1040638720985242.

82. Peng, Y., Zhang, H.W., Cao, W.H., Mao, Y., and Cheng, R.C. (2020). Exploration of the potential Biomarkers of papillary thyroid cancer (PTC) based on RT(2) profiler PCR arrays and bioinformatics analysis. Cancer Manag. Res. *12*, 9235–9246. https://doi.org/10.2147/CMAR.S266473.

83. Berrebi, D., Bruscoli, S., Cohen, N., Foussat, A., Migliorati, G., Bouchet-Delbos, L., Maillot, M.C., Portier, A., Couderc, J., Galanaud, P., et al. (2003). Synthesis of glucocorticoid-induced leucine zipper (GILZ) by macrophages: an anti-inflammatory and immunosuppressive mechanism shared by glucocorticoids and IL-10. Blood *101*, 729–738. https://doi.org/10.1182/blood-2002-02-0538.

84. Cohen, N., Mouly, E., Hamdi, H., Maillot, M.C., Pallardy, M., Godot, V., Capel, F., Balian, A., Naveau, S., Galanaud, P., et al. (2006). GILZ expression in human dendritic cells redirects their maturation and prevents antigen-specific T lymphocyte response. Blood *107*, 2037–2044. https://doi.org/10.1182/blood-2005-07-2760.

85. Siegel, P.M., and Massagué, J. (2003). Cytostatic and apoptotic actions of TGF-beta in homeostasis and cancer. Nat. Rev. Cancer *3*, 807–821. https://doi.org/10.1038/nrc1208.

86. Siegel, P.M., Shu, W., Cardiff, R.D., Muller, W.J., and Massagué, J. (2003). Transforming growth factor beta signaling impairs Neu-induced mammary tumorigenesis while promoting pulmonary metastasis. Proc. Natl. Acad. Sci. USA *100*, 8430–8435. https://doi.org/10.1073/pnas.0932636100.

87. Song, K.D., Kim, D.J., Lee, J.E., Yun, C.H., and Lee, W.K. (2012). KLF10, transforming growth factor-beta-inducible early gene 1, acts as a tumor suppressor. Biochem. Biophys. Res. Commun. *419*, 388–394. https://doi.org/10.1016/j.bbrc.2012.02.032.

88. Zhang, X., Yao, Y., Wei, W.Z., Yang, Z.Q., Gu, J., and Zhou, L. (2017). Impaired epidermal Langerhans cell maturation in TGFbeta-inducible early gene 1 (TIEG1) knockout mice. Oncotarget *8*, 112875–112882. https://doi.org/10.18632/oncotarget.22843.

89. Bagchi, D.P., Forss, I., Mandrup, S., and MacDougald, O.A. (2018). SnapShot: Niche determines adipocyte character I. Cell Metab. *27*, 264–264.e1. https://doi.org/10.1016/j.cmet.2017.11.012.

90. Tchkonia, T., Thomou, T., Zhu, Y., Karagiannides, I., Pothoulakis, C., Jensen, M.D., and Kirkland, J.L. (2013). Mechanisms and metabolic implications of regional differences among fat depots. Cell Metab. *17*, 644–656. https://doi.org/10.1016/j.cmet.2013.03.008.

91. Wernstedt Asterholm, I., Tao, C., Morley, T.S., Wang, Q.A., Delgado-Lopez, F., Wang, Z.V., and Scherer, P.E. (2014). Adipocyte inflammation is essential for healthy adipose tissue expansion and remodeling. Cell Metab. *20*, 103–118. https://doi.org/10.1016/j.cmet.2014.05.005.

92. Chang, M.C., Eslami, Z., Ennis, M., and Goodwin, P.J. (2021). Crown-like structures in breast adipose tissue of breast cancer patients: associations with CD68 expression, obesity, metabolic factors and prognosis. NPJ Breast Cancer *7*, 97. https://doi.org/10.1038/s41523-021-00304-x.

93. Agnoli, C., Grioni, S., Pala, V., Allione, A., Matullo, G., Gaetano, C.D., Tagliabue, G., Sieri, S., and Krogh, V. (2017). Biomarkers of inflammation and breast cancer risk: a case-control study nested in the EPIC-Varese cohort. Sci. Rep. *7*, 12708. https://doi.org/10.1038/s41598-017-12703-x.

94. Carter, J.M., Hoskin, T.L., Pena, M.A., Brahmbhatt, R., Winham, S.J., Frost, M.H., Stallings-Mann, M., Radisky, D.C., Knutson, K.L., Visscher, D.W., and Degnim, A.C. (2018). Macrophagic "Crown-like structures" are associated with an increased risk of breast cancer in Benign breast disease. Cancer Prev. Res. *11*, 113–119. https://doi.org/10.1158/1940-6207.CAPR-17-0245.

95. White, A.J., Nichols, H.B., Bradshaw, P.T., and Sandler, D.P. (2015). Overall and central adiposity and breast cancer risk in the Sister Study. Cancer *121*, 3700–3708. https://doi.org/10.1002/cncr.29552.

96. Neuhouser, M.L., Aragaki, A.K., Prentice, R.L., Manson, J.E., Chlebowski, R., Carty, C.L., Ochs-Balcom, H.M., Thomson, C.A., Caan, B.J., Tinker, L.F., et al. (2015). Overweight, obesity, and Postmenopausal Invasive breast cancer risk: asecondary analysis of the Women's Health Initiative randomized clinical trials. JAMA Oncol. *1*, 611–621. https://doi.org/10.1001/jamaoncol.2015.1546.

97. Macis, D., Aristarco, V., Johansson, H., Guerrieri-Gonzaga, A., Raimondi, S., Lazzeroni, M., Sestak, I., Cuzick, J., DeCensi, A., Bonanni, B., and Gandini, S. (2021). A novel Automated Immunoassay platform to evaluate the association of adiponectin and leptin levels with breast cancer risk. Cancers *13*, 3303. https://doi.org/10.3390/cancers13133303.

98. Oshi, M., Tokumaru, Y., Angarita, F.A., Lee, L., Yan, L., Matsuyama, R., Endo, I., and Takabe, K. (2021). Adipogenesis in triple-negative breast cancer is associated with unfavorable tumor immune microenvironment and with worse survival. Sci. Rep. *11*, 12541. https://doi.org/10.1038/s41598-021-91897-7.

99. Winter, J.M., Gildea, D.E., Andreas, J.P., Gatti, D.M., Williams, K.A., Lee, M., Hu, Y., Zhang, S.; NISC Comparative Sequencing Program, and Mullikin, J.C., et al. (2017). Mapping complex traits in a diversity outbred F1 mouse population identifies Germline Modifiers of metastasis in human prostate cancer. Cell Syst. *4*, 31–45.e6. https://doi.org/10.1016/j.cels.2016.10.018.

100. Yang, C., Wang, Y., Xu, W., Liu, Z., Zhou, S., Zhang, M., and Cui, D. (2019). Genome-wide association study using diversity outcross mice identified candidate genes of pancreatic cancer. Genomics *111*, 1882–1888. https://doi.org/10.1016/j.ygeno.2018.12.011.

101. Jacob, J., Radkevich, O., Forni, G., Zielinski, J., Shim, D., Jones, R.F., and Wei, W.Z. (2006). Activity of DNA vaccines encoding self or heterologous Her-2/neu in Her-2 or neu transgenic mice. Cell. Immunol. *240*, 96–106. https://doi.org/10.1016/j.cellimm.2006.07.002.

102. Andersson, S., Davis, D.L., Dahlbäck, H., Jörnvall, H., and Russell, D.W. (1989). Cloning, structure, and expression of the mitochondrial cytochrome P-450 sterol 26-hydroxylase, a bile acid biosynthetic enzyme. J. Biol. Chem. *264*, 8222–8229.

103. Xie, Z., Bailey, A., Kuleshov, M.V., Clarke, D.J.B., Evangelista, J.E., Jenkins, S.L., Lachmann, A., Wojciechowicz, M.L., Kropiwnicki, E., Jagodnik, K.M., et al. (2021). Gene set knowledge discovery with Enrichr. Curr. Protoc. *1*, e90. https://doi.org/10.1002/cpz1.90.

104. Tabula Muris Consortium, Supplemental text writing group, Principal investigators, Overall coordination, Logistical coordination, Organ collection and processing, Library preparation and sequencing, Computational data analysis, Cell type annotation, Writing group (2018). Single-cell transcriptomics of 20 mouse organs creates a Tabula Muris. Nature *562*, 367–372. https://doi.org/10.1038/s41586-018-0590-4.

105. McCarthy, C.E., White, J.M., Viola, N.T., and Gibson, H.M. (2020). In vivo imaging Technologies to monitor the immune system. Front. Immunol. *11*, 1067. https://doi.org/10.3389/fimmu.2020.01067.

106. Jacob, J.B., Kong, Y.c.M., Nalbantoglu, I., Snower, D.P., and Wei, W.Z. (2009). Tumor regression following DNA vaccination and regulatory T cell depletion in neu transgenic mice leads to an increased risk for autoimmunity. J. Immunol. *182*, 5873–5881. https://doi.org/10.4049/jimmunol.0804074.

107. Boggio, K., Nicoletti, G., Di Carlo, E., Cavallo, F., Landuzzi, L., Melani, C., Giovarelli, M., Rossi, I., Nanni, P., De Giovanni, C., et al. (1998). Interleukin 12-mediated prevention of spontaneous mammary adenocarcinomas in two lines of Her-2/neu transgenic mice. J. Exp. Med. *188*, 589–596. https://doi.org/10.1084/jem.188.3.589.

108. Lucchini, F., Sacco, M.G., Hu, N., Villa, A., Brown, J., Cesano, L., Mangiarini, L., Rindi, G., Kindl, S., Sessa, F., et al. (1992). Early and multifocal tumors in breast, salivary, harderian and epididymal tissues developed in MMTY-Neu transgenic mice. Cancer Lett. *64*, 203–209. https://doi.org/10.1016/0304-3835(92)90044-v.

109. Zhou, L., Adrianto, I., Wang, J., Wu, X., Datta, I., and Mi, Q.S. (2020). Single-cell RNA-seq analysis Uncovers distinct functional human NKT cell Sub-populations in peripheral blood. Front. Cell Dev. Biol. *8*, 384. https://doi.org/10.3389/fcell.2020.00384.

110. Radkevich-Brown, O., Piechocki, M.P., Back, J.B., Weise, A.M., Pilon-Thomas, S., and Wei, W.Z. (2010). Intratumoral DNA electroporation induces anti-tumor immunity and tumor regression. Cancer Immunol. Immunother. *59*, 409–417. https://doi.org/10.1007/s00262-009-0760-1.

111. Morgan, A.P., Fu, C.P., Kao, C.Y., Welsh, C.E., Didion, J.P., Yadgary, L., Hyacinth, L., Ferris, M.T., Bell, T.A., Miller, D.R., et al. (2015). The mouse Universal genotyping array: from Substrains to Subspecies. G3 (Bethesda) *6*, 263–279. https://doi.org/10.1534/g3.115.022087.

112. Broman, K.W., Wu, H., Sen, S., and Churchill, G.A. (2003). R/qtl: QTL mapping in experimental crosses. Bioinformatics *19*, 889–890. https://doi.org/10.1093/bioinformatics/btg112.

113. Svenson, K.L., Gatti, D.M., Valdar, W., Welsh, C.E., Cheng, R., Chesler, E.J., Palmer, A.A., McMillan, L., and Churchill, G.A. (2012). High-resolution genetic mapping using the Mouse Diversity outbred population. Genetics *190*, 437–447. https://doi.org/10.1534/genetics.111.132597.

114. Drebin, J.A., Stern, D.F., Link, V.C., Weinberg, R.A., and Greene, M.I. (1984). Monoclonal antibodies identify a cell-surface antigen associated with an activated cellular oncogene. Nature *312*, 545–548.

115. Sen, S., and Churchill, G.A. (2001). A statistical framework for quantitative trait mapping. Genetics *159*, 371–387.

116. Dunn, O.J. (1961). Multiple Comparisons among means. J. Am. Stat. Assoc. *56*, 52–64. https://doi.org/10.1080/01621459.1961.10482090.

117. Goeman, J.J., and Solari, A. (2014). Multiple hypothesis testing in genomics. Stat. Med. *33*, 1946–1978. https://doi.org/10.1002/sim.6082.

118. Bonferroni, C.E. (1936). Teoria statistica delle classi e calcolo delle probabilità (Pubblcazioni del R Instituto Superiore di Scienze Economiche e Commerciali di Firenze).

STAR★METHODS

KEY RESOURCES TABLE

REAGENT or RESOURCE	SOURCE	IDENTIFIER
Antibodies		
7.16.4 (anti-neu)	Millipore EMD	RRID:AB_2246567
CD45-APC	BioLegend	RRID:AB_2876537
PE-goat-anti-mouse IgG	Jackson ImmunoResearch	RRID:AB_2338629
IFN-gamma capture	BD Biosciences	RRID:AB_395387
IFN-gamma detection	BD Biosciences	RRID:AB_395374
Chemicals, peptides, and recombinant proteins		
AEC substrate	BD Biosciences	Cat#551951
Collagenase D	Millipore Sigma	Cat#11088858001
Collagenasetype 2	Worthington Biochemicals	Cat#LS004176
Deoxyribonuclease I	Sigma-Aldrich	Cat#D4263_5VL
RBC lysis buffer	ThermoFisher	Cat#00-4300-54
Debris removal kit	Miltenyi Biotec	Cat#130-109-398
TRIZOL reagent	ThermoFisher	Cat#15596018
Recombinent HER2-ECD-Fc protein	SinoBiological	Cat#10004-H02H
Critical commercial assays		
Next GEM single cell 3′ reagent kit	10X Genomics	Cat#1000121
ProtoScript II first strand cDNA synthesis kit	New England Biolabs	Cat#E6560S
iTaq universal SYBR Green supermix	Bio-Rad Laboratories	Cat#1725120
GigaMUGA	Neogen	Cat#550
Deposited data		
Mouse genomic data	UCSC Genome Browser, mm10	https://genome.ucsc.edu/index.html
Mouse strain gene polymorphism and insertions/deletions	Sanger Mouse SNP viewer (*no longer available*)	www.sanger.ac.uk/sanger/Mouse_SnpViewer Redirected as: https://www.mousegenomes.org
Ingenuity Pathway Analysis (IPA)	Qiagen	https://www.qiagen.com/us/products/discovery-and-translational-research/next-generation-sequencing/informatics-and-data/interpretation-content-databases/ingenuity-pathway-analysis/
Single cell RNA sequencing libraries	NCBI sequence read archive (SRA)	RPJNA929714
R code for QTL analysis and single cell analysis	Zenodo	https://doi.org/10.5281/zenodo.7059111
Experimental models: Cell lines		
E0771/E2	Radkevich-Brown et al.[28]	RRID:CVCL_GR23
Experimental models: Organisms/strains		
C57BL/6:C57BL/6NCrl	Charles River	RRID:IMSR_CRL:027
HER2 Tg:B6.Cg-*Pds5b*$^{Tg(WAP\text{-}ERBB2)229Wzw}$/J	Jackson Laboratories	RRID:IMSR_JAX:010562
BALB/c:BALB/cJ	Jackson Laboratories	RRID:IMSR_JAX:000651
Diversity Outbred (DO):J:DO	Jackson Laboratories	RRID:IMSR_JAX:009376
PWK:PWK/PhJ	Jackson Laboratories	RRID:IMSR_JAX:003715
C57BL/6 TIEG1-/-:TIEG1 knock-out	Gift from Dr. V. Poojary	N/A

(*Continued on next page*)

Continued

REAGENT or RESOURCE	SOURCE	IDENTIFIER
Oligonucleotides		
Neu-forward: ATCGGTGATGTCGGCGATAT	ThermoFisher	N/A
Neu-reverse: GTAACACAGGCAGATGTAGG	ThermoFisher	N/A
mTIEG1-forward: GTCTC AGTGCTCCCGTCTGT	ThermoFisher	Subramaniam et al.[5]
mTIEG1-reverse: CCACCG CTTCAAAGTCACTC	ThermoFisher	Subramaniam et al.[5]
mGAPDH-forward: CGTC CCGTAGACAAAATGGT	ThermoFisher	Subramaniam et al.[5]
mGAPDH-reverse: TCAATGA AGGGGTCGTTGAT	ThermoFisher	Subramaniam et al.[5]
Recombinant DNA		
pCMV5/E2TM; extracellular and transmembrane portions of human ERBB2/HER2	Generated in-house	Jacob et al.[101]
pCVM5	Gift of Dr. D.W. Russell, UT Southwestern	Andersson et al.[102]
Software and algorithms		
Cellranger	10X Genomics	https://support.10xgenomics.com/single-cell-gene-expression/software/pipelines/latest/what-is-cell-ranger
Seurat	Dorrity et al.[25]	https://satijalab.org/seurat/index.html
R	N/A	https://www.r-project.org
Rstudio	Posit	https://www.rstudio.com/products/rstudio/
EnrichR	Xie et al.[103]	https://maayanlab.cloud/EnrichR/
Tabula Muris	Tabula Muris et al.[104]	https://tabula-muris.ds.czbiohub.org
Venny	N/A	https://www.biotools.fr/misc/venny
Reactome	N/A	https://reactome.org
R/qtl2	Broman et al.[36]; Gatti et al.[34]	https://rqtl.org/qtl2cran
Expasy	N/A	www.expasy.org/translate
Enl database	N/A	www.enl.org
FlowJo	N/A	https://www.flowjo.com/solutions/flowjo
CodeAI	Caris Life Sciences	Proprietary
Other		
[^{64}Cu]Cu-NOTA-IgG	McCarthy et al.[105]	N/A
ELISPOT plates	Millipore Sigma	Cat#MSIPS4W10

RESOURCE AVAILABILITY

Lead contact

Further information and requests for resources and materials should be directed to and will be fulfilled by the lead contact, Wei-Zen Wei (weiw@karmanos.org).

Materials availability

This study did not generate new unique reagents.

Data and code availability

- The datasets analyzed during the current study are available from open access databases. Accession numbers are listed in the key resources table, Deposited Data section, NCBI SRA ID PRJNA929714.

- All original code has been deposited at Zenodo and is publicly available as of the date of publication. DOIs are listed in the key resources table in the Deposited Data section, ID: 10.5281/zenodo.7059111.
- Real world breast cancer survival data reported in this study cannot be deposited in a public repository because of rights of ownership. To request access, contact Joanne Xiu (jxiu@carisls.com).
- Any additional information required to reanalyze the data reported in this paper is available from the lead contact upon request.

EXPERIMENTAL MODEL AND SUBJECT DETAILS

All animal procedures were conducted in accordance with the U.S. Public Health Service Policy on Use of Laboratory Animals and with approval by Wayne State University Institutional Animal Care and Use Committee.

B6 HER2 Tg mice

Eight weekold C57BL/6 female were purchased from Charles River Laboratory and bred with C57BL/6 (B6) males carrying a single copy of the human ERBB2 (HER2) transgene under the WAP promoter.[27] The line was maintained by breeding HER2 positive males with B6 females. These mice to not develop spontaneous mammary tumors and are cared for in standard animal housing.

B6 TIEG1$^{-/-}$HER2 Tg mice

Eight weekold C57BL/6 female mice were purchased from Charles River Laboratory and maintained in the Animal Facility for breeding with male C57BL/6 TIEG1$^{-/-}$ mice (a gift from Dr. V. Poojary) to generate B6 HER2/TIEG1$^{+/-}$ F1 mice. To generate HER2/TIEG1$^{-/-}$ mice, F1 mice were backcrossed into B6 TIEG1$^{-/-}$ mice. These mice do not develop spontaneous mammary tumors.

BALB NeuT mice

Six to eight weekold female BALB/c mice were purchased from Jackson Labs to breed with BALB NeuT male mice carrying a single copy of activated rat neu, the homologue of human ERBB2.[23] Mice were maintained in standard animal housing. Female NeuT-expressing mice develop spontaneous mammary tumors beginning ~14 weeks of age and were palpated beginning at 10 weeks of age.

(BALBxB6) TIEG1$^{-/-}$ NeuT mice

BALB NeuT male mice were bred with B6 TIEG1$^{-/-}$ mice to generate (BALBxB6) TIEG1$^{+/-}$ NeuT F1 mice. F1 NeuT$^{+/-}$, TIEG1$^{+/-}$ male mice were then backcrossed to female B6 TIEG1$^{-/-}$ mice to generate (BALBxB6) TIEG1$^{-/-}$ NeuT mice. Mice were housed in standard animal housing. Female mice were palpated for spontaneous tumor development beginning at 10 weeks of age.

(BALBxDO) F1 NeuT mice

Eight to ten weekold female Diversity Outbred (DO) mice were purchased from Jackson Laboratories (strain DO:J) and bred with BALB NeuT male mice to generate (BALBxDO) F1 NeuT mice. Mice were maintained in standard housing and palpated for spontaneous tumor development beginning at 8 weeks of age to capture possible early spontaneous mammary tumors.

E0771/E2 cell line

E0771/E2 cells are on the C57BL/6 background and were provided by Dr. Daniel Allendorf (James Graham Brown Cancer Center, Louisville, KY). E0771/E2 were generated by transfecting E0771 with HER2[28] and are maintained in culture in SDME media with 10% fetal calf serum containing 500μg/ml neomycin. Mice were implanted in the flank with 2x10^5 cells in 100μl sterile phosphate buffered saline.

Tumor growth in BALB NeuT mice

BALB NeuT mice (provided by G. Forni and F. Cavallo, University of Torino, Torino, Italy, federica.cavallo@unito.it) were maintained in our facility by mating male NeuT mice with 6-8 weekold female BALB/c mice.[106] Homozygous Neu$^{+/+}$ mice die *in utero*, thus the presence of the remaining copy of the NeuT transgene was determined with PCR (primers listed in key resources table) from 0.5 cm of tail tissue when pups were 21 days of age.[107,108]

Tumor growth was monitored by palpation and measured with a vernier caliper two to three times per week. Tumor volume was calculated with the formula $XY^2/2$ where X is the long axis and Y is the short axis of the tumor. Tumor onset time is defined as the age of the mouse when the total volume of all spontaneous tumors reaches 63 mm^3. To model tumor growth rate, a differential equation was used to model the dynamical behavior of the tumor growth in time.[37] The typical trajectory of tumor growth consisted of an initial 'rise' period, followed by a 'rapid' exponential growth period (Figure 3A). Euthanization was required before the growth rate had plateaued. Thistype of growth rate is highly nonlinear and not a scaler constant. A differential equation was used to model the dynamical behavior of tumor growth in time (Equation 1).[37] The change in tumor volume is governed by a dynamic mechanism over time 't'. The equation incorporates both the autonomous cell division rate $c_1V(t)$ and an external driving force $c_2f(t)$ to accommodate treatment intervention as the study progresses.

The result is a first-order differential equation,

$$\frac{dV(t)}{dt} = c_1V(t) + c_2f(t) \quad \text{(Equation 1)}$$

where '$V(t)$' denotes the tumor volume which is a function of time 't'; 'c_1' is a proportional constant or growth rate determined from the tumor growth data. $f(t)$ denotes an external driving force, also a function of time 't'. It can be used to model the impact of immune attack, treatment response, etc. 'c_2' is a scaler constant. When 'c_2' takes a value of 0, it denotes an absence of an external driving force (thus autonomous tumor growth), while a value of 1 denotes the application of an external force $f(t)$.

In the autonomous mode when $c_2 = 0$, the solution of the differential Equation 1 has a closed form,

$$V(t) = e^{(c_1t + c_0)} \quad \text{(Equation 2)}$$

where 'e' is the natural exponent (or Euler's number) with a value of 2.7182, and c_0 is an offset constant. c_0 and c_1 are determined from the experimental data. When 'c_1' is positive, Equation 2 models a growing tumor; when c_1 is a negative value, Equation 2 describes a shrinking tumor. In general, 'c_1'can be a time-varying function to model complex interactions within the tumor. In this study, 'c_1' is a positive constant that represents tumor growth rate.

Taking a natural logarithm transformation of the total volume, Equation 2 converts the original exponential growth curve into a linear function of 't', as shown in Equation 3.

$$Ln(V) = c_1t + c_0 \quad \text{(Equation 3)}$$

$Ln(V)$ becomes a linear function in time 't' with a constant slope 'c_1'. The region of exponential growth was identified empirically from the tumor size data and the slope c_1 of $Ln(V)$ was calculated from the slope of the trend line of the $Ln(V)$data for each mouse.

ImmunoPET tumor imaging

BALB NeuT mice bearing spontaneous mammary tumors were injected i.v. in the lateral tail vein with [^{64}Cu] Cu-NOTA-α-Neu (~180–240 μCi/mouse, 42.8–57.1 μg in 150 μL sterile saline, clone 7.16.4) or control [^{64}Cu] Cu-NOTA-IgG.[105] Imaging was acquired from 4 to 72 hours post injection (p.i.). The animals were anesthetized with 3-5% isoflurane (Baxter Healthcare) in air for induction, then lowered to 1.5% to 2% for maintenance. Images were acquired with a microPET R4 camera (Siemens Medical Solutions, USA, formerly Concorde Microsystems). Manually drawn three-dimensional volumes of interest (VOI) were selected to determine maximum and mean percent injected dose per gram (%ID/g) in target tissues. Images were decay-corrected to the time of injection and analyzed for tracer uptake using ASIpro VMTM software v. 6.3.3.0.

Single cell RNA (scRNA-Seq) analysis

Single cell transcriptome libraries of whole mammary fat pad or mammary tumor tissue were generated. Lymph nodes embedded in #4 and #9 fat pads were removed before fat pads were harvested and pooled.[35] Spontaneous tumors at 65-300 mm^3 without visible necrosis were dissected out without surrounding mammary fat pad tissue as the source of the 'tumor' scRNA-Seq library. Mammary tissue surrounding tumor tissue was collected for generation of an 'adjacent' library. Tissue was minced finely with scalpels and enzymatically dissociated (4mM $NaHCO_3$, 0.01M HEPES, 2.5mg/ml Collagenase D [Millipore Sigma, Burlington,

MA] and 5mg/ml Collagenasetype 2 [Worthington-Biochemical, Lakewood, NJ] in RPMI media). Following filtration (70mm filter [Miltenyi Biotech, Auburn, CA]) and washing (500x*g* for 10 minutes), red blood cells were lysed utilizing RBC lysis buffer (ThermoFisher, Waltham, MA) and debris removed using the debris removal kit (Miltenyi Biotech, Auburn, CA), per the manufacturer's protocol. Samples with viability above ~90% proceeded to single cell library construction using the 10X Genomics Chromium Next GEM Single Cell 3' Reagent kit (v3.1 chemistry) and Chromium Single Cell Controller per the manufacturer's instructions (https/assets.ctfassets.net/an68im79xiti/1eX2FPdpeCgnCJtw4fj9Hx/7cb84edaa9eca04b607f9193162994de/CG000204_ChromiumNextGEMSingleCell3_v3.1_Rev_D).[109] cDNA libraries were sequenced (NextSeq 500, Illumina, San Diego, CA) to a saturation of 60-70%, with an average of 50,000 UMI counts/cell at the Center for Molecular Medicine and Genetics Genomics Core, Wayne State University. Reads were demultiplexed, aligned to the refdata-cellranger-mm10-2020-A, barcodes processed and UMI counts obtained using 10X Genomics' Cell Ranger version 4.0.0.

The transcript profiles of cell clusters were integrated and analyzed using the R-based package Seurat v4.0.6 (https://satijalab.org/seurat/index.html) using UMAP dimensional reduction with a resolution of 0.3.[25,26] Fold change values, heatmaps, dotplots and top gene IDs were generated using Seurat. Cluster identity was made by using the top 5 genes as input to EnrichR[103] and verified using Tabula Muris.[104] The Venn diagram was generated utilizing Venny (https://www.biotools.fr/misc/venny) and unique pathways using reactome (https://reactome.org).

Mouse model: TIEG1$^{-/-}$

All animal procedures were conducted in accordance with the U.S. Public Health Service Policy on Use of Laboratory Animals and with approval by Wayne State University Institutional Animal Care and Use Committee.

Generation of HER2/TIEG1 knock-out mice was performed by crossing C57BL/6 TIEG1$^{-/-}$ mice (provided by Dr. Venuprasad Poojary) with C57BL/6 (B6) mice purchased from Charles River Laboratory (RRID in key resources table). B6 HER2/TIEG1$^{+/-}$ mice were generated by crossing B6 HER2 Tg mice (B6.Cg-*Pds5b*$^{Tg(WAP-ERBB2)229Wzw}$/J in key resources table) with B6 TIEG1$^{-/-}$. Mice carrying the HER2 transgene were then backcrossed to B6 TIEG1$^{-/-}$ to generate B6 HER2/TIEG1$^{-/-}$ mice. B6 HER2/TIEG1$^{-/-}$ mice were electro-vaccinated intramuscularly (im, ep) with 50μg plasmid DNA encoding the extracellular and transmembrane portions of human ERBB2 (pE2TM)(sequence has been reported in[101]) and mouse 20μg GM-CSF (pGM-CSF)(provided by Dr. N. Nishisaki at Osaka University, Osaka, Japan). The blank vector, pCMV5,[102] was the control.

Following vaccination, B6/HER2 and B6/HER2/TIEG1$^{-/-}$ mice were challenged with HER2-expressing mammary E0771/E2 cells. E0771/E2 cells were provided by Dr. Daniel Allendorf (James Graham Brown Cancer Center, Louisville, KY) and were generated by transfecting E0771 with HER2.[28] Tumor growth was monitored by palpation and measured with a vernier caliper two to three times per week. Tumor volume was calculated with the formula $XY^2/2$ where X is the long axis and Y is the short axis of the tumor.

To generate NeuT/TIEG1 knockout mice, BALB NeuT mice were crossed with B6 TIEG1$^{-/-}$ mice to generate (BALBxB6) F1 NeuT/TIEG1$^{+/-}$ mice, which were then backcrossed with B6 TIEG1$^{-/-}$ mice to generate (BALBxB6) B1 NeuT/TIEG1$^{-/-}$ mice. Tumor growth was monitored as for B6/HER2/TIEG1$^{-/-}$ or NeuT, as above.

HER2-specific T cell response

HER2 reactive T cells were enumerated by IFN-γ ELISPOT.[29,110] IFN-γ ELISPOT reagents were purchased from BD Biosciences. Spleens were harvested at 6 weeks following the last pE2TM vaccination and dissociated to form single cells. Splenocytes were incubated in ELISPOT plates coated with IFN-γ capture mAb for 48 hrs with recombinant HER2 protein (ecd-Fc fusion; SinoBiological). Biotinylated IFN-γ detection mAb was added for 2 hours and AEC substrate added to develop the spots. Results were expressed as the number of cytokine-producing cells per 10^6 SC. Data were analyzed using the student's *t* test.

qPCR analysis of TIEG1 expression

Real-time qPCR of mouse TIEG1 in TIEG1$^{+/-}$ and TIEG1$^{-/-}$ NeuT mice. Tumor tissue samples were snap frozen in liquid nitrogen, total RNA isolated using Trizol reagent (ThermoFisher), and cDNA synthesized

with ProtoScript II First Strand cDNA Synthesis kit (New England Biolabs). TIEG1 expression was determined using real-time qPCR performed with iTaq Universal SYBR Green Supermix (Bio-Rad Laboratories) as recommended by the manufacturer. Mouse GAPDH (mGAPDH) RNA was amplified simultaneously in each reaction. Relative TIEG1 expression was calculated using the ΔΔCt method, compared to GAPDH. Primers for mTIEG1 and mGAPDH are listed in the key resources table.

Mouse model: Diversity outbred NeuT F1

DO mice (J:DO, stock #009376) were purchased from the Jackson Laboratory. BALB NeuT mice were maintained in our facility by mating male NeuT mice with female BALB/c mice as described above.[106] NeuT male mice were bred with DO female mice to generate (BALBxDO) F1 NeuT negative and (BALBxDO) F1 NeuT heterozygous (referred to as NeuT) mice. All $NeuT^{+/-}$ mice were monitored for tumor onset and growth. Tumor growth was monitored by palpation and measured with a vernier caliper two to three times per week. Tumor volume was calculated with the formula $XY^2/2$ where X is the long axis and Y is the short axis of the tumor. Tumor onset time was defined as the age of the mouse when the total volume of all spontaneous tumors reaches 63 mm^3. Two NeuT female mice per litter were randomly selected for genetic linkage analysis. Tumor onset in male NeuT mice was also observed but linkage analysis is not reported here due to low mouse numbers.

The PWK strain drives aggressive tumors

We collaborated with Jackson Laboratories to mate female PWK/PhJ mice with heterozygous male BALB NeuT mice at the Jackson Laboratory to generate (BALBxPWK) F1 NeuT mice. Tumor onset and growth was monitored in our animal care facility from the age of 5 wks, as described.

Mouse genotyping and QTL analysis

The genotype of each test (BALBxDO) F1 NeuT mouse was determined using the Giga Mouse Universal Genotyping Array (GigaMUGA), built on the Illumina Infinium platform.[111] The assay is performed centrally at Neogen. https://genomics.neogen.com/en/mouse-universal-genotyping-array.

DO QTL or the later R/qtl2 software package was used to calculate genotype probabilities from GigaMUGA with a hidden Markov Model that generates a probabilistic estimate of the diplotype state at each marker locus in each DO animal and evaluates the association between genotype and phenotype (https://rqtl.org/qtl2cran).[34,36,112,113] Genotyping data for the DO founders are available at https://www.jax.org/research-and-faculty/genetic-diversity-initiative/tools-data/diversity-outbred-reference-data. DO mice carry 36 possible diplotypes while (BALBxDO) F1 mice have only 8 possible haplotypes in addition to the BALB/c haplotype. With 8 degrees of freedom in the genome scan analysis, the F1 model has a greater probability of detecting QTLs than the DO model with 36 degrees of freedom.

Analysis of the impact of SNP

Published literature (NCBI protein) and publicly available databases (USCS Genome Browser; Sangar mouse SNP Viewer) (FigureS2) were utilized to determine changes in amino acids. Specific changes to DNA were identified using the Sangar mouse database, protein reading frame determined by Expasy analysis (www.expasy.org/translate) and verified using NCBI Nucleotide and BLAST databases. The location of binding motifs was identified using the Enl database (www.enl.org).

Real-world database analysis

We queried the deidentified real-world evidence (RWE) dataset from the Caris Life Sciences using CODEai, a real-word clinic-genomic data platform that integrates patient's molecular data with cancer treatment and clinical information obtained from insurance claims data.[38] Breast cancer patients with whole transcriptome sequencing performed on mRNA isolated from a formalin-fixed paraffin-embedded tumor sample using the Illumina NovaSeq platform (Illumina, Inc., San Diego, CA) were included in the analysis. Cohorts included 4,920 patients with metastatic disease and 3,568 patients with primary tumors. RWE overall survival (rwOS) was calculated for all cases, which was defined as time of tissue collection date to either death or last contact in the insurance claims repository. As previously reported, patient death was assumed for any patient without a claim for more than 100 days, which holds true for more than 95% of patients with a recorded death in the NDI (National Death Index).[39] Cases were grouped by expression of individual

genes. The 26 heritable cancer risk genes were compared in patients with greater than median normalized gene expression to those with less than median normalized gene expression.

Network analysis

A list of candidate genes was generated and used as input to query Ingenuity Pathway Analysis (IPA). The Network Analysis tool was used to identify candidate genes which influenced similar genes.

Flow cytometry

BALB NeuT tumors were enzymatically dissociated using the enzymatic digestion buffer described in the scRNA-Seq method (above) and stained using mAb 7.16.4 (Millipore) to detect rat neu epitope[114] and APC-conjugated CD45 (BioLend). PE-goat-anti-mouse IgG (Jackson ImmunoResearch Laboratories, Inc., West Grove, PA) was the secondary Ab. Samples were analyzed on a BD FACScanto II using FlowJo v10.5 software (TreeStar, Ashland OR).

QUANTIFICATION AND STATISTICAL ANALYSIS

Murine tumor-free survival was graphically summarized using Kaplan-Meijer curves and compared using the log-rank test with a $p<0.05$ considered significant. Differences in Ab concentration and IFN-γ-secreting T cells were analyzed using a paired student's *t* test.

Support intervals for DO QTL localization were determined using a 95% Bayesian credible interval.[115] The logarithm of the odds (LOD) curve is transformed by raising it to the power of 10 and a region covering 95% of the area under the transformed curve defines the support interval. The area under the curve is numerically approximated using trapezoids between the marker loci. Allele association was inferred by the strain influence on the QTL. Alleles were examined using the SNP viewer: www.sanger.ac.uk/sanger/Mouse_SnpViewer and filtered on the consensus regions.

In the real world overall survival (rwOS) analysis, the survival outcomes were compared between groups using the log-rank test and the corresponding *p*-value was corrected for multiplicity using Bonferroni correction.[116–118]